A diffusion tensor imaging study in HIV patients with and without apathy

by
Jean-Paul Fouche

Thesis presented in fulfilment of the requirements for the degree of
Master of Medical Physiology at the
University of Stellenbosch.

Supervisor: Dr. Bruce Shawn Spottiswoode
Co-supervisors: Prof. Hans Strijdom & Dr. Paul Dermot Carey
Faculty of Health Sciences
Department of Medical Physiology

December 2010

Declaration

By submitting this thesis/dissertation electronically, I declare that the entirety of the work contained therein is my own, original work, and that I have not previously in its entirety or in part submitted it for obtaining any qualification.

December 2010

Abstract

HIV/AIDS is a global epidemic that accounts for a large percentage of the mortality in South Africa every year. Since the implementation of anti-retroviral treatment, HIV positive individuals have been living longer, and the cognitive impairment associated with the disease is becoming increasingly apparent. During the initial systemic infection of HIV, the virus migrates through the blood-brain barrier and inflicts axonal injury by causing upregulation of cytokines and neurotoxic proteins. HIV-associated dementia is a neuropsychological classification of cognitive impairment in HIV and a variety of symptoms have been classified as a part of the dementia complex. One of these is apathy, which is thought to be a precursor for dementia in HIV patients. Three groups of individuals have been recruited and scanned using magnetic resonance imaging (MRI) to examine changes in the brain. These are an HIV non-apathetic cohort, an HIV apathetic cohort and a healthy control cohort. Diffusion tensor imaging (DTI) is an MRI technique used to quantitatively assess white matter (WM) integrity using metrics such as fractional anisotropy (FA). Voxel-based analysis, tract-based spatial statistics (TBSS) and tractography are three established DTI analysis methods that have been applied in numerous studies. However, there are certain methodological strengths and limitations associated with each technique and therefore all three of these techniques were used to compare WM differences across groups. The frontal-subcortical pathways are known to be abnormal in apathy, and this has been demonstrated in a number of imaging studies. Most of these studies have examined apathy in the context of neurodegenerative disorders such as Alzheimer's disease and Parkinson's. However, to our knowledge this is the first DTI study in HIV apathetic patients. With the tractography method, the anterior thalamic radiation and the corpus callosum were reconstructed for each individual to determine whether there were any global changes in these tracts. No significant changes were found. However, a variety of regions in the WM were significantly abnormal in the HIV cohorts when comparing the data at a voxel-based level and using TBSS. This included areas such as the genu and splenium of the corpus callosum, the internal capsule and corona radiata. Changes in frontal WM for the HIV apathy group are an indication of dysfunction in the frontal-striatal circuits, and previous literature has implicated these circuits in the neuropathology of apathy in a variety of central nervous system (CNS) disorders.

Uittreksel

MIV/VIGS is `n wêreldwye epidemie wat verantwoordelik is vir `n hoë sterftesyfer in Suid-Afrika elke jaar. Sedert die inleiding van anti-retrovirale behandeling, het die MIV-positiewe populasie se lewensduur verleng. Tesame met langer lewensduur, het die kognitiewe verswakking wat geassosieer word met die siekte ook meer prominent na vore gekom. Gedurende die beginstadium van sistemiese infeksie in MIV is daar `n migrasie van die virus deur die bloed-breinskans. MIV kan indirek verantwoordelik wees vir aksonale beskadiging deur verhoging van neurotoksiese proteine en sitokinien te induseer. MIV-geassosieerde demensie is `n neurosielkundige klassifikasie van kognitiewe verswakking in MIV en verskeie simptome is al geïdentifiseer as deel van die demensie kompleks. Een van die simptome is apatie en daar word gespekuleer dat dit `n voorloper is vir demensie in MIV pasiënte. Drie groepe individue was gewerf vir die studie en geskandeer deur magnetiese resonansie beeldvorming (MRB) om sodoende veranderinge in die brein te ondersoek. Die groepe was onderskeidelik `n HIV nie-apatiese kohort, `n HIV apatiese kohort en `n gesonde kontrole kohort. Diffusie tensor beelding (DTB) is `n MRB tegniek wat toegepas word om witstof integriteit te meet deur gebruik te maak van maatstawwe soos fraksionele anisotropie (FA). “Voxel-based analysis”, “tract-based spatial statistics (TBSS)” en “tractography” is drie gevestigde DTB analitiese metodes wat al in talle studies toegepas was. Daar is egter sekere metodologiese voordele en beperkings verbonde aan elke tegniek en daarom is al drie tegnieke gebruik om witstof verskille tussen groepe te vergelyk. Die frontale-subkortikale roetes in die brein is bekend vir abnormaliteite in apatie en dit was ook al gedemonstreer in verskeie studies. Die meeste van die studies het apatie ondersoek in die konteks van neuro-degeneratiewe siektes soos Alzheimer se siekte en Parkinson se siekte. Maar sover ons weet is hierdie die eerste DTB studie in MIV pasiënte met apatie. Met die “tractography” metode was die *anterior thalamic radiation* en *corpus callosum* herbou vir elke individu. Dit was om te bepaal of daar enige globale veranderinge is in hierdie gebiede, maar geen beduidende veranderinge is gevind nie.`n Verskeidenheid van gebiede in die witstof was beduidend abnormaal in die MIV kohorte wanneer die data vergelyk was met “TBSS” en “voxel-based analysis.” Dit het gebiede ingesluit soos die *genu* en *splenium* van die *corpus callosum*, die *internal capsule* en die *corona radiata*. Veranderinge in die frontale witstof vir die MIV-apatie groep is `n aanduiding van disfunksie in die frontale-striatale bane. Vorige literatuur impliseer dat hierdie bane betrokke is in die neuro-patologie van apatie in verskeie sentrale senuweestelsel (SS) steurings

Acknowledgements

Firstly I would like to thank Dr. Paul Carey and Dr. Bruce Spottiswoode for giving me the opportunity to learn a variety of imaging analyses and being able to run the EEG lab at CUBIC. Especially Bruce who was always willing to help me out if I got stuck with the technical details, I lost count of the number of times I would knock at his office door with a big question mark across my face. Paul, thank you for the chance to work on numerous projects and gain invaluable experience in the field of neuroscience and the guidance you have always shown me. It has been a very educational experience and it has given me the necessary know-how to be able to contribute to the neuroimaging community in South Africa.

And secondly to all the staff at CUBIC a heartfelt thanks for being so accommodating and showing me the ropes. Every person here has volunteered their own expertise and has helped me gain an understanding of the techniques and science of brain imaging in all its associated facets. The team here at CUBIC are phenomenal people and I am proud to be part of the group here as we all contribute in our own way. Also thanks to Dr. Strijdom and the physiology department for giving me the platform on which to do this thesis, and also for his guidance regarding the scientific process and proposal.

Thirdly I dedicate this to my fiancée, Debbie Jones who has supported me in this endeavour from the moment I decided to do my MSc and whom I love dearly. Even in my neurotic and stressful times she was there with a kind word and encouragement. And also my family and friends who were there for me in the good and the bad times, thanks to all!

Lastly but not least, I would also like to acknowledge Siemens Medical Solutions for providing the MRI facilities and equipment.

Contents

List of figures and tables

Nomenclature

DTI: diffusion tensor imaging

MRI: magnetic resonance imaging

WM: white matter

FA: fractional anisotropy

GM: grey matter

ADC: apparent diffusion coefficient

MD: mean diffusion

RD: radial diffusivity

AD: axial diffusivity

TBSS: tract-based spatial statistics

VBM: voxel-based morphometry

ATR: anterior thalamic radiation

CC: corpus callosum

BBB: blood-brain barrier

CNS: central nervous system

APP: amyloid precursor protein

MPT: membrane permeability transition

SPECT: single photon emission computed tomography

PD: proton density

TE: echo time

CSF: cerebrospinal fluid

IVIM: intra-voxel incoherent motion

DWI: diffusion-weighted imaging

ROI: region of interest

HAART: highly active anti-retroviral therapy

IHDS: International HIV Dementia Scale

DSM-IV: Diagnostic and Statistical Manual of Mental Disorders 4th edition

MINI: Mini International Neuropsychiatric Interview

ELISA: enzyme-linked immunosorbent assay

AES: apathy evaluation scale

TR: repetition time

SPM: statistical parametric mapping

FSL: FMRIB Software Library

MNI: Montreal Neurological Institute

ANOVA: analysis of variance

FMRIB: Oxford Centre for Functional Magnetic Resonance Imaging of the Brain

BET: brain extraction toolkit

GLM: general linear model

FACT: Fiber Assignment by Continuous Tracking

SPSS: Statistical Package for the Social Sciences

SCR: superior corona radiata

CST: corticospinal tract

ACR: anterior corona radiata

PCR: posterior corona radiata

ALIC: anterior limb of the internal capsule

CP: cerebral peduncle

EC: external capsule

MCP: middle cerebellar peduncle

SCP: superior cerebellar peduncle

PLIC: posterior limb of the internal capsule

SLF: superior longitudinal fasciculus

SS: sagittal stratum

DOF: degrees of freedom

1. Introduction

HIV is thought to enter the brain early in the course of infection via the blood-brain barrier and then accumulate in the basal ganglia (Haase et al., 1986). Initially there is no cognitive impairment, but eventual cognitive deterioration is evident later in the disease and is characterised by neuropsychiatric dysfunctions such as loss of psychomotor speed, memory, motor skills and learning capacity with co-morbid behavioural symptoms such as apathy and depression (Lawrence et al., 2001). The underlying pathogenesis of cognitive impairment is unknown at this stage, but it has been speculated that activation of the microglia and/or brain macrophages, along with the release of inflammatory cytokines and chemokines could be a causal factor leading to abnormal pruning (Mori et al., 2003). Evidence of CNS axonal injury has also been demonstrated by immunohistochemistry staining techniques (Gray et al., 1998; Adle-Biassette et al., 1999).

The presence of HIV-related axonal injury in subcortical white matter, the accumulation of HIV in the basal ganglia and the detrimental brain inflammation due to viral proteins and cytokine release, have prompted research into the effects of HIV on brain structure and function. Various techniques have been used to study the structure of the human brain as well as its physiological and pathological processes. Histology staining techniques and electron microscopy has been previously applied in animal models and post-mortem human brains to determine the locations of proteins and genes of interest on a molecular level. However, methods like these are labour-intensive and not useful for studying *in-vivo* pathological processes of diseases such as HIV in the human brain (Mori et al., 2006).

Magnetic resonance imaging (MRI) is being used more frequently for *in vivo* brain imaging research, and it has supplied the research community with a variety of tools to study the structure, physiology and function of the human brain. Diffusion tensor imaging (DTI) is a relatively new MRI technique which is capable of studying the local diffusion properties of white matter (Basser et al., 1994). DTI measures water diffusion, or random thermal motion, in a variety of different directions and uses this to estimate white matter (WM) tract orientation. In WM, the direction of water diffusion follows the path of least resistance, thus along the axonal membranes and fibers. Because of this characteristic, diffusion measured in WM is anisotropic, with random water movement oriented largely parallel to the fibers. Fractional anisotropy (FA), which indirectly represents the co-linearity of WM fibers, can be derived from DTI measurements and is a useful metric of WM integrity (Pierpaoli et al.,

1996). The FA value is measured on a scale of 0 to 1, with 1 representing the highest theoretical level of WM co-linearity (approached by major WM tracts) and values approaching 0 representing isotropic diffusion (such as grey matter). Abnormalities in WM lead to a decrease of FA (the reason for this will be explained in Chapter 2.4). However, to acquire a better picture of what is happening at a microstructural level, it is important to examine a number of other diffusion parameters. Other parameters include the mean diffusivity (MD), radial diffusitivity (RD) and axial diffusitivity (AD). RD and AD are more specific to demyelination and axonal damage, respectively, as shown by previous animal studies (Song et al., 2002; Song et al., 2003). MD, as the name implies, is the mean diffusion in all directions, and is indicative of inflammation in brain regions.

The DTI technique can be applied to patients with HIV to examine the underlying WM microstructural pathology. This can give an indication of axonal injury, loss of white matter integrity and inflammation due to CNS infection in HIV^+. Of particular interest here is the study of apathy in a HIV^+ population. Apathy is clinically defined as a reduction in self-initiated cognitive, emotional and behavioural activity with features that can present similarly to depression. Apathy has been shown to occur in conjunction with a variety of neurological syndromes, such as Parkinson's disease, Alzheimer's and negative-syndrome schizophrenia (Andreasen et al., 1982; Starkstein et al., 1992; Ott et al., 1996). It has also been suggested that working memory deficits occur in HIV patients presenting with apathy (Castellon et al., 1998).

The focus of this work is thus to examine WM changes occurring in a South African HIV positive (HIV^+) population with and without apathy by comparing diffusion-derived measures of this population with the corresponding measures in a healthy control group. DTI changes between apathetic and non-apathetic HIV^+ patients will be examined to isolate changes related to apathy.

The four DTI-derived measurements (MD, FA, AD and RD) are compared across the three subject groups using tract-based spatial statistics (TBSS) (Smith et al., 2006) and an analysis method based on voxel-based morphometry (VBM) (Ashburner et al., 2000). In addition to these whole-brain techniques, there will also be a focus on specific WM regions (such as frontal WM and the corpus callosum) that are known to cause apathy in individuals when these structures are compromised. The anterior thalamic radiation (ATR) and corpus callosum

(CC) are reconstructed by fiber tracking methods and the FA of the tracts is compared across the groups.

In Chapter 2.1 and 2.2, the physiological and neuropsychiatric changes associated with HIV will be explained, specifically relating to cognitive impairments and the damage caused by the virus in axonal membranes. Chapter 2.3 introduces the concept of apathy in neuropsychiatric disorders with a focus on neuroimaging done to examine this phenomenon in a variety of diseases. Current concepts about the manifestation of apathy in HIV are also conveyed. Chapter 2.4 provides an overview of DTI, as well as the physiology underlying this modality. Chapter 2.5 reviews the literature on previous DTI studies that have been performed in HIV^+ cohorts, emphasizing the lack of DTI studies in apathy associated with HIV. Chapter 3 details the analysis methods employed in this study and Chapter 4 presents the results obtained using these techniques. Chapters 5 and 6 will discuss the implications of the findings as well as the limitations of this study.

2. Background

2.1 Infection of the brain by HIV

Neurological symptoms are common in patients with HIV/AIDS and a variety of clinical symptoms have been observed, namely cognitive impairments, motor speed abnormalities and behavioural changes such as apathy and depression (Lawrence et al., 2002). Certain cases of neurological diseases are a result of opportunistic infection because of immunodeficiency; however, in the absence of these infections an estimated 20-30% of HIV^+ individuals will develop neurocognitive defects such as HIV dementia (Gray et al., 1998). Autopsy findings of patients with HIV have also demonstrated focused groups of microglia, macrophages and multinucleated giant cells (Gray et al., 1998). It is intriguing that neurons are not the target of the infection; there is even some evidence that a patients' condition can improve after treatment with delay of further neurocognitive deterioration (Lawrence et al., 2002). This suggests that nerve cell loss is unlikely to be the main contributing factor to HIV-associated neurological changes.

Crossing the blood-brain barrier

In Fig 2.1 the process of HIV invasion through the blood-brain barrier (BBB) is demonstrated. The BBB is a selectively permeable membrane which is important for regulating the transfer of substances between the brain tissue and blood vessels. However HIV-1 enters through the BBB via mechanisms that have recently been identified in animal models in vitro (Gonzalez-Scarano et al., 2005). One model for this process is the Trojan horse hypothesis (demonstrated in Fig 2.1). This model proposes that the HIV virus invades the brain using cells as vehicles for entry. Immune cells that become infected, such as T cells and monocytes, can thus enter the BBB and cause propagation of the virus in the central nervous system (CNS) (Haase et al., 1986). Another hypothesis for entry of the virus into the CNS is that the virus can migrate between endothelial cells of the BBB microvasculature, thus providing a method of direct entry into brain tissue (Kramer-Hammerle et al., 2005). In theory all of the main cell types of the CNS can be infected by HIV, as all of these cells possess co-receptors necessary for HIV entry, but in reality macrophages and microglia are infected the most (Gonzalez-Scarano et al., 2005). However this does not exclude the possible infection of other CNS cells, such as astrocytes and oligodendrocytes. The macrophage population comprise the resident immune cells of the brain which reside close to the peripheral blood vessels of the brain. These cells have a short lifespan with a quick turnover, probably because they are located close to the

peripheral vessels of the brain. The macrophages are replaced by the migration of monocytes into the brain, and it is by this mechanism that infected monocytes cross the BBB. These monocytes can then differentiate into macrophages, and together with microglia the virus can be propagated by the infected immune cells (Anderson et al., 2002; Kaul et al., 2001).

Astrocytes and olygodendrocytes are the supporting cells of WM and these cells can also be infected by HIV. Although these cells possess certain co-receptors for binding with the HIV virus, there is no CD4 receptor on the cell membranes which is required for binding and infection by HIV. Even so reports have indicated that there is viral attachment via mechanisms that are unclear at this point (Gorry et al., 2003; Neumann et al., 2001). Although certain studies have reported viral nucleic acids in situ for these cells (Nuovo et al., 1994; Bagasra et al., 1996) it is still debatable whether the WM supporting cells are involved in the propagation of the virus in the CNS to the same degree as that of the microglia and macrophages.

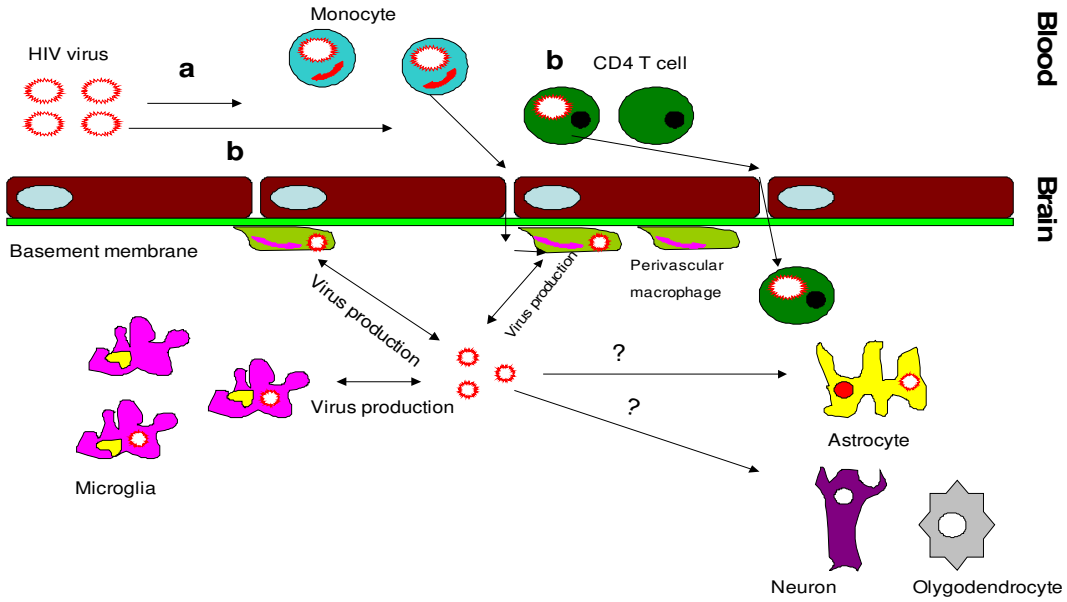

Fig 2.1: The infection of HIV crossing the blood-brain barrier (BBB). In (a) the virus binds with CD4 receptors on the monocyte that cross the BBB and differentiate into macrophages which are in turn involved in virus production together with microglia. (b) Another method of invasion is via the CD4 T cells of the immune system. It is unknown whether the virus can infect neurons, astrocytes and/or oligodendrocytes, although certain in situ studies have demonstrated viral nucleic replication (Nuovo et al., 1994; Bagasra et al., 1996).

Axonal injury in HIV

Amyloid precursor protein (APP) immunohistochemistry is a method which reveals regions of axonal injury in AIDS and HIV patients. This staining method detects accumulated APP proteins during impaired fast axonal transport, which is indicative of axonal injury or insult. These APP-positive axons (APP^+) have been found predominantly in subcortical white matter, basal ganglia and the brainstem of HIV patients in association with microglia/macrophages and multinucleated giant cells (Gray et al., 1998; Adle-Biassette et al., 1999). Another possible correlate with axonal injury is diffuse myelin pallor as this is a common autopsy finding in patients with HIV encephalopathy. A relationship between APP^+ axons and diffuse myelin pallor has been demonstrated in these studies (Raja et al., 1997). However, axonal injury has also been described in the absence of myelin pathology in a HIV patient who died after displaying symptoms of relapsing neurological signs. In this case study, the patient predominantly showed signs of axonal damage without any other neuropathological changes (Gray et al., 1998). Using a simian model of HIV, Mankowski and colleagues have also demonstrated increased APP^+ axons in the absence of diffuse myelin pallor (Mankowski et al., 2002). These studies suggest that axonal injury is the primary physiological manifestation of HIV infection in the brain, and therefore it is important to examine the mechanisms of axonal injury in HIV/AIDS.

Mechanisms of axonal injury

Increased axonal membrane permeability is expected as a result of neuroinflammation, energy deficits, and acidosis associated with the CNS infection. Thus there is increased Na^+ and Ca^{2+} inside the axon which can cause changes at the axolemma (LoPachin et al., 1994). Ca^{2+} is the mediator in axonal injury and degeneration. Because of calcium overloading, the mitochondrial membrane permeability transition (MPT) pores of the axonal mitochondria become permeable for small molecules, and this process leads to an uptake of water with subsequent mitochondrial swelling and rupture. This in turn causes the release of cytochrome c which is associated with caspase activation in the axon (Buki et al., 2000). The caspases destroy the intra-axonal cytoskeleton and organelles. One of the major effects of the caspases on the axon cytoskeleton is the cleavage of intra-axonal spectrin, which ultimately destroys the cytoskeleton, an event that transpires in various CNS disorders (Wang et al., 1998). A specific caspase, namely caspase-3 also cleaves calpastatin, which is an inhibitor of calpain.

Calpain acts on a number of substrate molecules, of which cytoskeletal proteins such as spectrin and other neurofilament proteins are part of this group (Buki et al., 2000; Wang et al., 1998). This breakdown in cytoskeletal structure can result in severe functional abnormalities in the axon that could ultimately affect neuronal function as well.

There are also mechanisms that can lead to indirect axonal damage. One example of this is the disruption of interactions between glial cells and neurons. These interactions are critical for maintaining brain homeostasis and are also vital for neuronal survival after brain injury. Glial cells can also be a source of neurotoxic factors which are produced in response to brain insult or infectious diseases (Giulian et al., 1993). Cytotoxic T cells, microglia and other macrophages have also been implicated in axonal injury, as well as T antibodies, metalloproteinases and other inflammatory molecules such as TNF-α and nitric oxide (Langford et al., 2001).

2.2 Neuropsychiatric changes during HIV infection

The insult to the CNS via the mechanisms described in the previous section result in a range of neuropsychiatric conditions and abnormal neuropsychological functioning in patients with HIV/AIDS. These conditions have been a focus of clinical research since the start of the epidemic. Individuals infected with HIV have exhibited a range of neuropsychiatric symptoms such as mania, anxiety and other psychotic disorders (Hinkin et al., 2001). Of these disorders, depression has been the most extensively studied in the HIV population, due to the high prevalence of depression in HIV. Another symptom that is reported more in HIV patients than the normal population is apathy (Hinkin et al., 2001). Apathy can be characterized as a reduction in cognitive, behavioural and emotional activity that is initiated by the self. Although many of the features overlap with that of depression, apathy is a distinctive phenomenon that can be identified in patient populations (Marin, 1990). HIV-associated dementia and apathy are also considered a potential attribute of the dementia complex, which is a condition displaying symptoms such as reduced psychomotor speed, poor concentration and memory impairment (Ho et al., 1989). However, apathy has also been reported in HIV patients without HIV dementia and with less severe disease progression. One example of this is a study by Paul and colleagues which reported that 26% of the HIV^+ population sample presented with clinically significant apathy and average CD4 cell counts of 300, indicative of less severe immunosuppression (Paul et al., 2005).

2.3 HIV and apathy

Neuroimaging of apathy in several diseases

Different brain regions have been associated with the pathophysiology of apathy in a variety of diseases. Apathy can be described as pathology of voluntary action, or more specifically, goal-directed behaviour. Therefore functional brain circuits involved with the execution and control of goal-directed behaviour are involved (Brown et al., 2000). This section highlights a number of brain abnormalities demonstrated in the imaging literature. Both grey and white matter regions are affected and display abnormally on MRI together with other studies showing decreased perfusion of brain blood vessels in single photon emission computed tomography (SPECT). The anterior cingulate has been implicated as a role-player in apathy. In SPECT studies of Alzheimer patients who presented with apathy, there was a significant negative correlation of neuropsychiatric apathy scores with right anterior cingulate activity, and bilateral cingulate activity reduction (Migneco et al., 2001). Case studies have suggested that the frontal grey matter brain regions are also affected in apathy. In another SPECT study, a patient who suffered from a thalamic stroke presented with signs of apathy and reduced perfusion in the bilateral frontal regions (McGilchrist et al., 1993). Reduced cerebral blood flow has also been demonstrated in the dorsolateral prefrontal cortex and in the left frontotemporal cortex in apathetic stroke patients (Okada et al., 1997). In another study Watanabe et al., (1995) observed decreased perfusion in bilateral frontal regions of a subcortical stroke patient. Several other SPECT studies have also indicated that the basal ganglia are involved (van Reekum et al., 2005). Evidence for subcortical atrophy has been demonstrated by volume reductions in subcortical regions such as the caudate and nucleus accumbens in MRI studies (Jernigan et al., 2005). A case study of an Alzheimer's patient with apathy revealed that there was decreased perfusion in the bilateral basal ganglia and the prefrontal cortex (Lopez et al., 2001). In 70 brain injury patients presenting with apathy, lesions have been detected in the grey matter subcortical structures as measured by CT, MRI and EEG (van Reekum et al., 2005). Also, in 80 apathetic stroke subjects, CT lesions have been detected in white matter regions, specifically the posterior limb of the internal capsule (Starkstein, 1992). This bundle of white matter fibers connects the parietal, temporal and occipital cortices of the brain to the thalamic regions.

The lesions described in the above mentioned studies are located in regions of the frontal-subcortical circuits (specifically the anterior cingulate and prefrontal cortex). Apathy has been

shown to be a feature of lesions or dysfunctions in frontal-subcortical structures due to a variety of brain disorders (Levy et al. 2006). However the biological evidence for apathy presenting in HIV has not been sufficiently explored, especially in white matter regions relevant to the frontal-subcortical circuits. Thus we hypothesize that when comparing the HIV apathetic cohort to a healthy control cohort, abnormalities in DTI are expected in white matter regions such as the anterior thalamic radiation, corpus callosum genu, anterior limb of the internal capsule and the posterior limb of the internal capsule. Figs 2.2 and 2.3 show the anatomical location of the aforementioned regions.

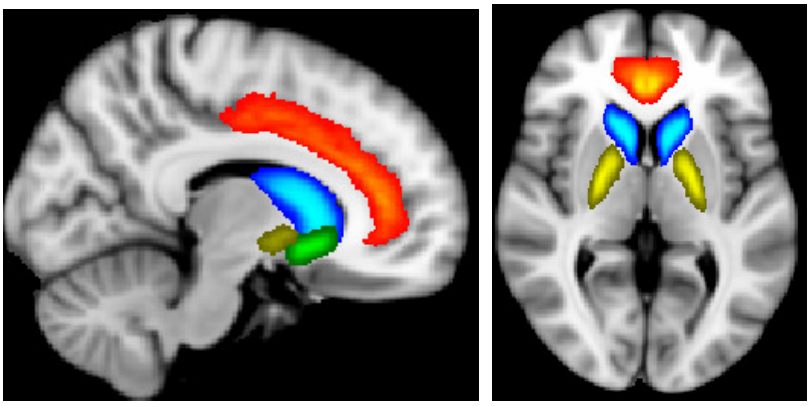

Fig 2.2: Grey matter regions associated with apathy as demonstrated in the literature. The colours correspond to the structures as follows: **yellow** – pallidum (part of the basal ganglia); **blue** – caudate; **green** – accumbens; **orange** – anterior cingulate. The image was acquired from the Harvard-Oxford cortical and subcortical structural atlases that are part of the FSL toolbox.

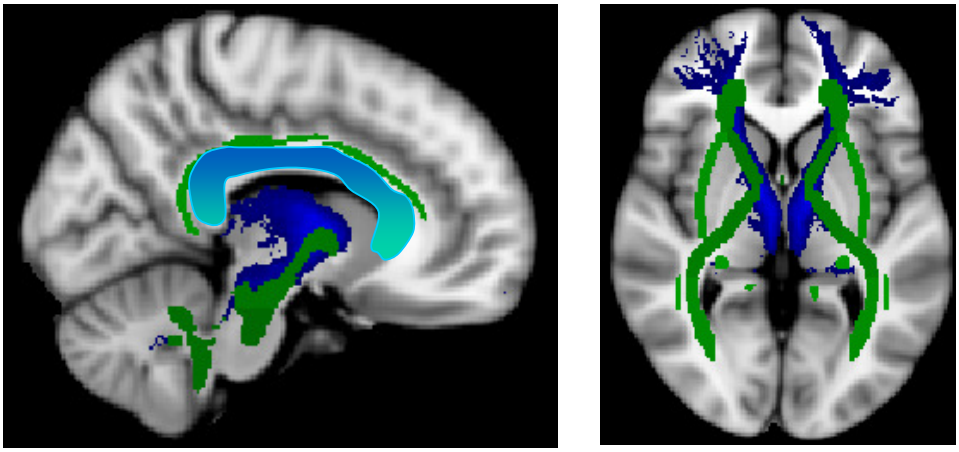

Fig 2.3: The white matter regions connecting frontal, parietal and subcortical structures of the brain. The following white matter tracts are hypothesized to be abnormal in the pathogenesis of apathy: the anterior thalamic radiation (blue), the anterior and posterior limbs of the internal capsule (green) and the genu of the corpus callosum (blue-green). Image was acquired from the JHU DTI-based white matter atlas that is part of the FSL toolbox.

HIV with apathy as a co-morbidity

At this stage it is still unknown whether apathy develops as a secondary condition because of the psychosocial demands of HIV or because of the actual basal ganglia infection of the disease. Given that the disease accumulates in the basal ganglia and other critical nuclei, the frontal-subcortical structures have been implicated in the development of apathy (Paul et al., 2005). It is known that that these structures may be important in the regulation of cognition, emotions and behaviour. Previous studies have found a positive correlation between the degree of apathy and the status of cognitive impairment in HIV patients (Castellon et al., 1998; Castellon et al., 2000). However, another study by Rabkin and colleagues did not find a correlation between these parameters (Rabkin et al., 2000). A study by Paul et al. (2005) shows that increased ratings of apathy correlated ($r = -0.59$, $p < 0.05$) with lower nucleus accumbens volume (the nucleus accumbens is a nuclei structure that is central to the anterior cingulate frontal circuit). The correlation of the ratings were acquired by the use of the Apathy Evaluation Scale (self-report version) which is an 18 item report with subjects needing to respond to a statement on a scale of 1-4 with 4 corresponding to total agreement and 1 to no agreement. A final score is then calculated which corresponds to the degree of apathy in a subject (Marin et al., 1991). Also in this specific study, ratings of depression had no significant effect on either the nucleus volume or apathy (Paul et al., 2005). These comparisons were between HIV^+ apathetic patients and normal controls and therefore factors other than apathy could be responsible for the changes.

2.4 Diffusion tensor imaging

Magnetic resonance imaging

Magnetic resonance imaging (MRI) is a non-invasive imaging modality that allows one to study the brain in its entirety. The MRI procedure is also non-invasive, and it doesn't require the introduction of radioactive isotopes or ionizing radiation as with other imaging modalities. MRI offers a variety of different tissue weighting methods which can be applied to examine different brain structures (Mori et al., 1999). Several important MRI concepts are required before introducing diffusion-weighted imaging, the technique used in this study. The signal measured by MRI emanates from hydrogen protons within tissues. Depending on the physical and chemical environments of protons in certain types of tissue, a variety of weighted images can be generated and the relative contrasts of differing tissue types can be used to outline certain major structures. In Fig 2.4 the difference between the contrasts are seen for common

clinical MRI sequences. Depending on the scan parameters, images highlighting white matter (T1-weighted) or grey matter (proton density and T2-weighted) can be acquired.

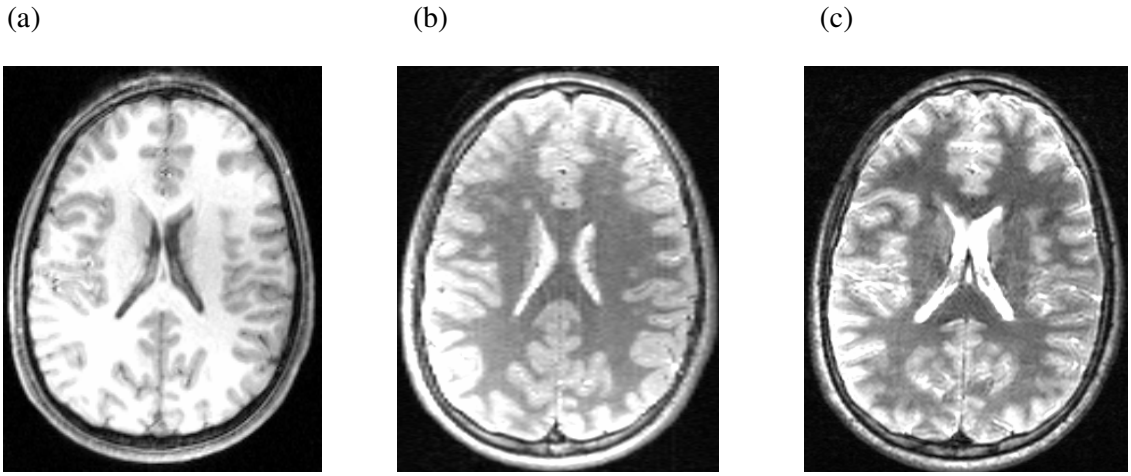

Fig 2.4: Three common MRI sequences showing a variety of contrasts between adjacent tissue. The images displayed here are a T1-weighted image (a), a proton density image (b) and a T2-weighted image (c) of the same subject.

Basic MRI physics

Fig 2.5 gives a graphical representation of the manipulation of water protons during the magnetic resonance imaging procedure. Protons in the human body rotate (or precess) around their own axes, and in the absence of an external magnetic field the directions of this precession is randomly orientated. As soon as a strong magnetic field is applied, the protons align with the field and are said to spin about this axis. In a standard proton density (PD) image the signal measured from these precessing protons is proportional to the concentration of water within the tissue being imaged. To measure this signal a radio frequency pulse is applied, causing the protons to lose alignment with the main magnetic field and subsequently emit radio waves specific to each tissue. These radio waves are then measured after the application of a series of magnetic field gradients, and used to reconstruct an image. Thus a PD image will display bright cerebrospinal fluid (which is 99% water) and darker white matter (which contains a large amount of fat and few free hydrogen atoms).

As an example, the acquisition of T2 and PD contrasts will be explained (Mori et al., 1999). After the excitation of protons by the magnetic field, the signal from the precessing protons will start to fade or “relax”. Thus T2 relaxation occurs, which is the loss of synchronization between the proton spins. The reason for this is that each proton starts to precess at different speeds due to the local non-homogeneity of the magnetic field after the initial excitation. T2-

weighting can be acquired by inserting a time delay between excitation and signal acquisition, namely the echo time (TE). Depending on TE, the degree of weighting will differ. Shorter echo times lead to acquisition of lightly weighted images (the PD being an example of that) and longer times lead to more heavily T2-weighted images. Different types of brain tissue produce different signal characteristics in T2-weighted images: regions displaying slower relaxation such as CSF appear brighter with WM and GM appearing darker because of faster relaxation. To construct the image from the raw data acquired by the scanner (which is usually a 256 x 256 matrix of data points known as k-space), processing is required in the form of Fourier transforms. These transforms calculate the magnitude of the radio-frequency waves emitted by proton spins at discrete spatial locations. The magnitude data can then be expanded to a data matrix of pixels which appear as a greyscale image (Hornak, 1996).

The conventional MRI methods are useful for determining the location and extent of pathologies in the brain, as well as delineating physical structures. Another type of image weighting is diffusion weighting. Here additional magnetic field gradients are used to vary the magnetic field in a linear direction. Because of these field variations, the protons will precess at different rates and result in a loss of overall signal. However, the second gradient is applied in the same direction but of opposite magnitude to refocus the precession of the protons. Thus, stationary protons will regain the signal lost while moving spins will exhibit a net signal loss. Using this technique, images can be sensitized for diffusion changes in brain tissues as described in the next section (Mori et al., 1999).

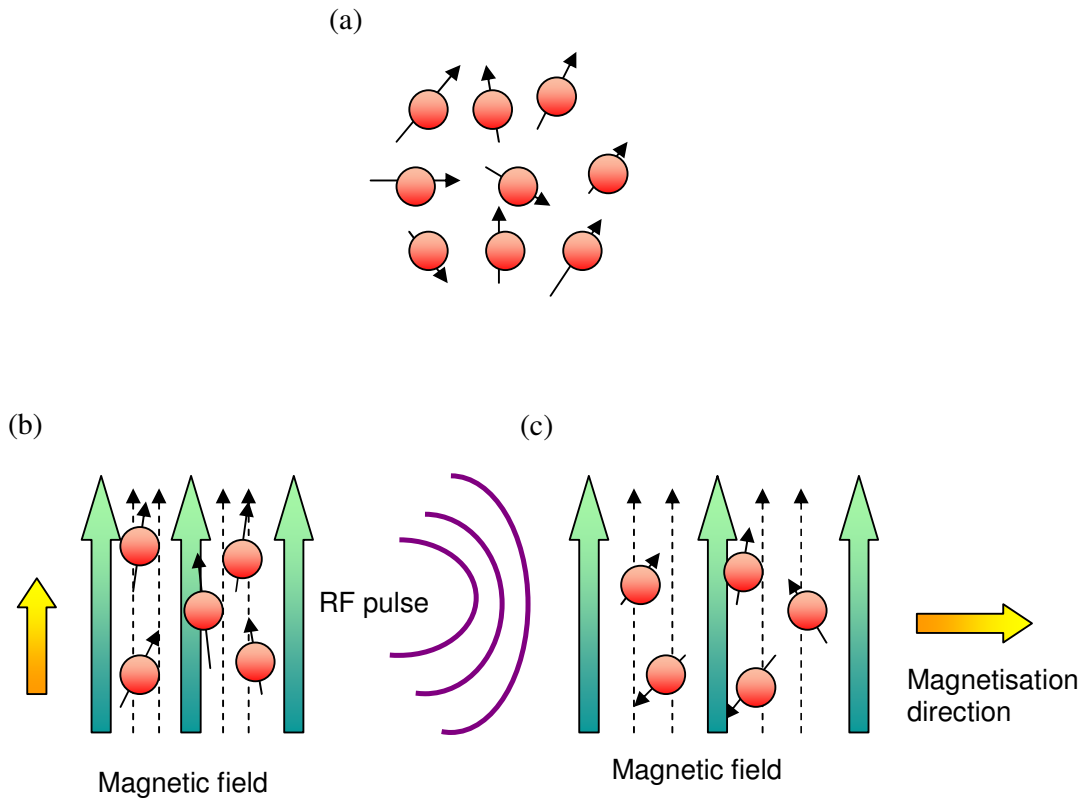

Fig 2.5: A demonstration of proton manipulation in an MRI scanner. (a) Water protons are usually randomly orientated when rotating about their own axes. (b) When applying a strong magnetic field, protons will align parallel to the field. (c) When a tuned radio frequency pulse is applied to protons in a magnetic field, the protons are knocked out of alignment with the magnetic field and radio frequency signals are then detected from this disturbance, leading to the MRI signal

Diffusion weighted imaging

LeBihan et al. (1986) designed the first DWI scan sequence in which diffusion sensitizing gradient field pulses were incorporated in order to measure a tissue contrast that is related to microscopic water displacement. Initially this was applied to measure the intravascular motion of water via the intravoxel incoherent motion (IVIM) method (LeBihan et al., 1986). However this method was not very successful as it was difficult to distinguish between the water signal in blood and tissue (Neil et al., 2008). Even so, scientists have found other uses for DWI, for example to detect acute stroke in patients (Moseley et al., 1990), or other research applications for examining WM differences across subject populations. As introduced above, DWI relies on the initial application of a gradient field pulse to dephase (or unwind) precessing protons, with a subsequent inverted gradient pulse to rephase (or rewind) the protons. The phase of stationary protons returns to its original value and a net phase accumulates for moving protons. The random water motion between gradient pulses thus

decreases the DWI signal (Neil et al., 2008). The motion of water in tissues can be influenced by a number of factors, such as molecular weight, viscosity, membrane microstructure and temperature. The latter is important for the movement of molecules in a fashion known as Brownian motion (the random thermal motion of water) (Neil et al., 2008). Depending on the region in the brain, the displacement of water will be different due to constriction of membranes (as in WM). These barriers constrict the diffusion and result in less signal loss, wheres areas with no barriers (e.g. CSF) have a large signal loss. DWI can be a reliable technique for detecting deterioration in WM before clinically significant lesions or volume reductions are apparent (Hall et al., 2004).

Diffusion eigenvectors/eigenvalues as a means of describing constrained water diffusion

As mentioned above, the cellular microstructure of tissue can influence the mobility of protons because of barriers to diffusion. Barriers to diffusion include boundaries between the different compartments of membranes and cells (for example extracellular and intracellular compartments, neurons, axons and glial cells). In highly-ordered structures such as WM, diffusion is restricted by axonal membranes and myelin sheaths. Water displacement can be categorized according to isotropic and anisotropic diffusion (Fig 2.6). This can be explained using the following analogy: When a drop of dye is placed into a large stationary container with water, the dye will diffuse out as an expanding sphere. This is called isotropic diffusion as the diffusion is the same in all directions. However, if a drop of dye were to be placed in the WM, the shape obtained after a while will resemble that of an ellipsoid or rugby ball. The long axis of the ellipse would then represent the direction of greatest diffusion in WM indicating that water displacement is the greatest along the fibers of WM, because diffusion is restricted by barriers in the perpendicular directions (Beaulieu et al., 2002). This is known as anisotropic diffusion, and a 3×3 matrix called a tensor can be used to describe these 3D ellipses.

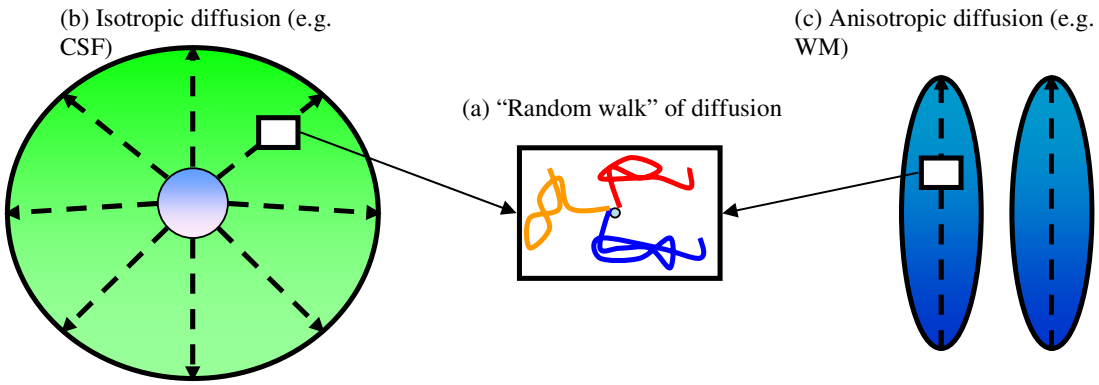

Fig 2.6: Isotropic and anisotropic diffusion. Water in living cells moves according to random thermal motion (Brownian motion). As indicated in (a) particles start diffusing at the same origin, but due to external factors such as heat and viscosity, diffusion is chaotic. However, in some tissues the mean displacement is restricted by compartments. Two examples of diffusion are shown here. (b) When molecules are in an open body of water their motion is equally probable in any direction and the diffusion is isotropic. (c) When water is contained in restrictive compartments (such as in WM), diffusion will occur in an anisotropic manner with preferential diffusion occurring along the axons.

When performing diffusion measurements in an MRI scanner, the operator of the scanner can determine in which direction the gradient field pulses are applied, and thus the direction in which water displacement is measured. The resulting diffusion measurement will be different for each direction. Seeing as the displacement of water varies with space, a number of different gradient directions are used make up the tensor matrices describing the diffusion characteristics for each voxel. This technique is known as diffusion tensor imaging (DTI). For the purposes of DTI, measurements should be made in at least 6 directions - the minimum required directions for a 3×3 tensor matrix describing orientation in three orthogonal directions. In practice, around 30-120 different gradient directions are typical. These images, in combination with a B0 image (a T2-weighted baseline image with identical image parameters but no diffusion weighting), are used to calculate a tensor matrix for each volume element (voxel) (Fig 2.7). Eigenvalue decomposition of this tensor (Llacer, 1982) results in three eigenvectors (λ_1, λ_2 and λ_3) and the corresponding eigenvalues (E1, E2 and E3). These eigenvalues describe the diffusion coefficient in each eigenvector direction. In myelinated WM (Fig 2.8) the primary eigenvector (λ_1) is in a direction parallel to the fibers, with the corresponding eigenvalue (E1) known as the axial diffusivity ($\lambda_{\parallel}$). The average of the other two eigenvalues (E2 and E3) is known as the radial diffusivity ($\lambda_{\perp}$) and the corresponding eigenvectors (λ_2 and λ_3) are perpendicular to the WM fiber direction (Basser et al., 1994). The physiological interpretation and importance of these parameters will be explained later.

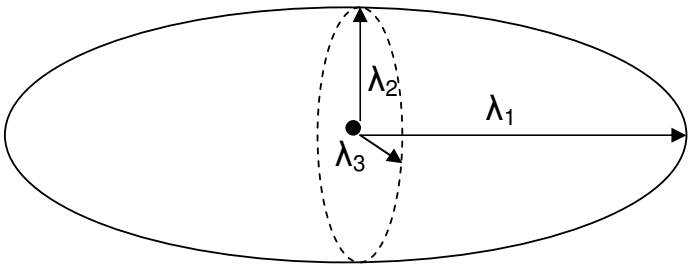

Fig 2.7: Eigenvalue decomposition of a tensor results in vectors that describe the principle axes of an ellipsoid. The principal diffusion direction (λ_1) or eigenvector 1 is usually aligned parallel to the axonal fibers in WM. The other two eigenvectors (λ_2 and λ_3) are in perpendicular directions to the fibers.

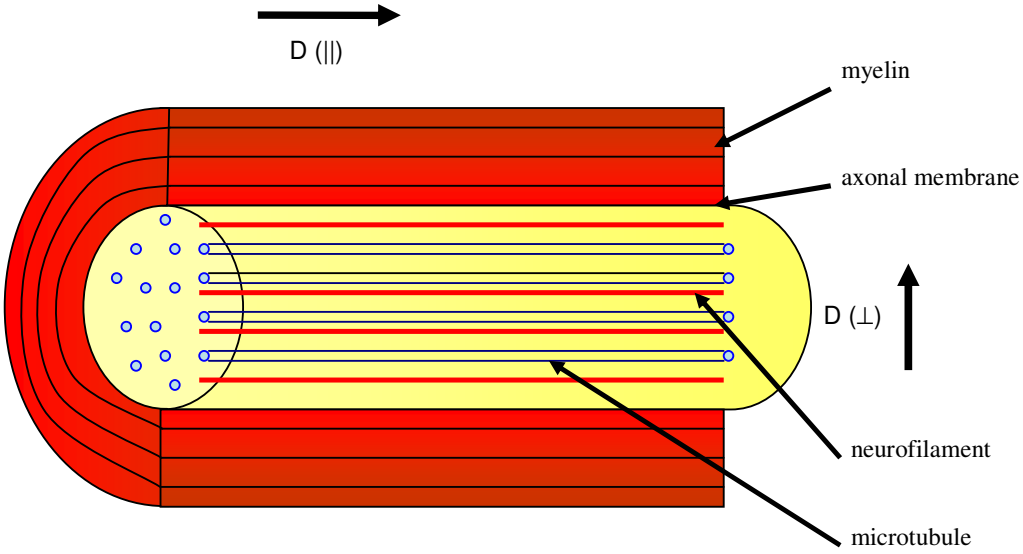

Fig 2.8: A representation of a myelinated axon, indicating diffusion in parallel (axial diffusion) and perpendicular (radial diffusion) directions.

Calculating FA and MD maps from the diffusion tensors

Fractional anisotropy (FA) and mean diffusivity (MD) are widely used metrics when comparing WM across different subject groups. The MD image of a subject can be calculated by determining the diffusion coefficient at each voxel of the MR image data (Basser et al., 2002). Mean diffusivity is calculated as follows:

$$\mathbf{MD} = \text{Trace}(D)/3$$
$$=(D_{xx} + D_{yy} + D_{zz})/3$$
$$= (\lambda_1 + \lambda_2 + \lambda_3)/3$$

The intensity of each pixel in the MD map is directly proportional to the amount of diffusion (D) within that specific region, thus bright regions (such as the CSF in Fig 2.4b) correspond to areas with high diffusion. Fractional anisotropy is more descriptive of white matter than MD as it provides a measure related to the collinearity of white matter fibers within a voxel. The degree of diffusion anisotropy can be calculated using a normalized difference measurement between the three eigenvalues:

$$\mathbf{FA} = \sqrt{\frac{(\lambda_1 - MD)^2 + (\lambda_2 - MD)^2 + (\lambda_3 - MD)^2}{2(\lambda_{1^2} + \lambda_{2^2} + \lambda_{3^2})}}$$

If diffusion is perfectly isotropic (thus $\lambda_1=\lambda_2=\lambda_3$), the FA measure will be 0 (Pierpaoli et al., 1996).This FA index is normalized between 0 (perfectly isotropic) and 1 (perfectly anisotropic). As shown in Fig 2.4, highly anisotropic structures (e.g. WM) have FA values approaching 1 and appear brighter, and more isotropic structures (e.g. grey matter or cerebrospinal fluid) appear darker. Statistical inference can be performed on group MD and FA values to determine whether there are structural abnormalities in WM.

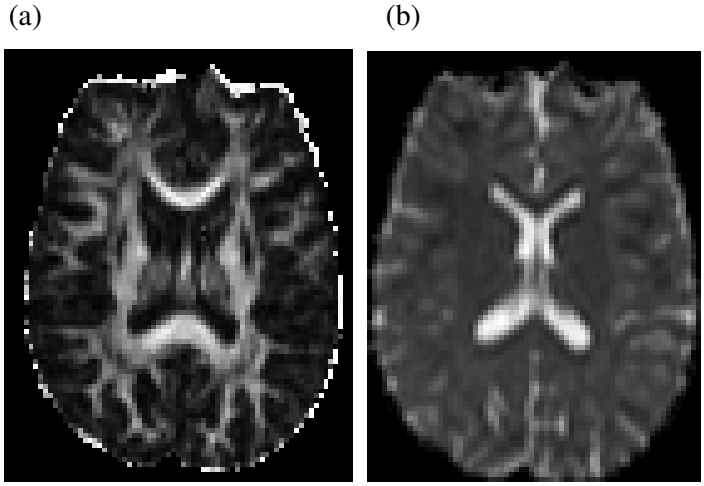

Fig 2.9: (a) Example fractional anisotropy (FA) image. The WM tracts appear brighter with other tissue being darker. (b) Corresponding MD image where the WM intensity is low, with GM and CSF appearing progressively brighter.

Physiological basis of diffusion anisotropy

As shown in Fig 2.8 axons have a unique structure with microtubules and neurofilaments that are responsible for fast axonal transport as well as an axonal membrane with a myelin sheath that is critical for successful signal transduction along the WM tracts.

A popular hypothesis for anisotropic water diffusion in WM is that perpendicular diffusion in axons is limited by the myelin sheaths encasing the axons, with the lipid bilayers of myelin thus hindering diffusion across axonal fibers (Beaulieu et al., 1994). One can thus infer that demyelinated fibers are less anisotropic because of the decreased resistance to water diffusion perpendicular to the direction of the axon. However, previous authors have observed anisotropic diffusion in normal non-myelinated nerves of the garfish (Beaulieu et al., 1994). The extent of anisotropy in these excised nerve samples was similar to human *in vivo* data and this study was one of the first to indicate that myelin is not an essential component for anisotropic diffusion in WM. However, this does not mean that myelin has no role in anisotropy, but rather that there are other structural characteristics of axons that can contribute to anisotropy. Demyelination is thus not the only source of decreased FA in human WM. These findings have been confirmed in other animal models such as the non-myelinated walking leg nerve of the lobster (Beaulieu et al., 2002) and the demyelinated WM of rat pups (Wimberger et al., 1995). A study by Gulani and colleagues has demonstrated that myelin can modulate the degree of anisotropy in a myelin-deficient Wistar rat model (Gulani et al., 2001). In these X-linked recessive rat mutants, Gulani et al. demonstrated that myelin can alter MD values. In this model, MD increased by 50% when compared to normal myelinated rats. The MD increase was also more significant in the perpendicular direction (75%) than the parallel direction (35%) which is to be expected with the loss of myelin. Although it is difficult to determine the contribution of myelin to diffusion anisotropy, it can be said that for two fiber tracts equal in axonal density and size, one myelinated and the other demyelinated, there would be greater diffusion anisotropy in the myelinated axons. It has also been observed that anisotropy increases as the brain develops, but whether this is because of WM myelination or greater fiber coherence remains to be seen (Sakuma et al., 1991).

Neurofibrils such as neurofilaments and microtubules could contribute to increased anisotropy as these structures can physically hinder perpendicular water diffusion. Beaulieu et al. examined this theory by measuring the axoplasm in an isolated giant squid axon in order to minimize the interference from the axonal membranes (Beaulieu et al., 1994). The diffusion

was anisotropic in the axoplasm, with a ratio (parallel/perpendicular) of 1.2. This also matched Monte Carlo computer simulations of randomly diffusing particles in a structure similar to the neurofilament cytoskeleton of the giant squid (Beaulieu et al., 1994). This study demonstrates that the neurofilaments do not play a significant role in anisotropy, and therefore axonal membranes and myelin are likely to be the primary determinants of anisotropy.

Physiological basis of axial and radial diffusivity

Recently, diffusion parameters other than FA and MD have been compared in a number of studies (Budde et al., 2007). As described in Section 4.5, the problem with comparing FA and MD data is that underlying mechanisms of WM abnormalities cannot be completely elucidated. As explained above, decreases in FA could be as a result of axonal damage or myelin degeneration. Further information can be gleaned by separating the directional diffusivities into components parallel (λ_1) and perpendicular (λ_2 and λ_3) to the axons. These components are known as the axial diffusivity (λ_1) and radial diffusivity ($\lambda_2 + \lambda_3$)/2, respectively (Budde et al., 2007). Previous studies in dysmyelinated rat models have indicated that changes in the diffusivities are specific to axonal or myelin degeneration. It has been shown by Song et al. 2002 that in a shiverer mouse model (where there is little to no myelin surrounding intact axons) axial diffusivity was not different to a control sample. However, the radial diffusivity was larger in the shiverer model which is an indication of the increased perpendicular motion of water across broken or non-existent myelin sheaths (Song et al., 2002). Song et al. (2005) found increased radial diffusivity after feeding male mice with cuprizone (a neurotoxin that interferes with the function of enzymes responsible for myelin maintenance and production) to induce demyelination of the corpus callosum (CC). Remyelination was achieved by stopping cuprizone treatment and resuming normal chow feeding, resulting in a decrease in radial diffusivity. Another study by Song et al. (2003) demonstrated differential outcomes of axonal and myelin damage in a mouse model of ischemia in the retina. After 3 days of retinal ischemia, decreased axial diffusivity was found in the optic nerve with no changes in radial diffusivity consistent with histological data. After 5 days, myelin degeneration occurred, with corresponding radial diffusivity increases and no axial diffusivity change. Therefore axial and radial diffusivity have been demonstrated to be specific markers for axonal and myelin degeneration, respectively.

2.5 White matter diffusion changes in HIV

A number of DTI studies have been performed to investigate abnormalities in FA and MD in patients with HIV. These parameters have also been correlated with neurological dysfunction, for example, dementia (Ragin et al., 2004). Filippi et al. (2001) found a correlation between viral load and the reduction of FA in the splenium and genu of the corpus callosum in 10 subjects with HIV. In another study by Pomara and colleagues, in a cohort of 6 HIV positive subjects, decreased FA was shown in frontal WM when compared to controls, but no differences were found in MD (Pomara et al., 2001). In both of these studies, regions of interest (ROI's) were outlined and diffusion measures were calculated from these ROI's. The average of these measures was then compared between groups to determine significant differences. However, with this type of method pre-defined ROI's need to be specified. Their method is also dependent on inter- and intra-rater variability, which is not the case with the automated approaches used in this study (see Section 3.3). Also, the diffusion measures are averaged across a large region of WM and therefore are not sensitive to more localized WM features. Even so, evidence for the detrimental effect of HIV on the WM was demonstrated, especially in dense fibers, such as in the corpus callosum.

Another study by Cloak et al. (2004) shows increased mean diffusivity in frontal WM, as well as increases in glial metabolites (indicating infection and inflammation in these areas). This was in a slightly larger cohort of 11 HIV subjects compared to 14 normal controls. The authors also found that the MD correlated positively with myoinositol (a glial marker) and therefore, this was an indication that mean diffusion increases are associated with inflammation (seeing as glial activation is associated with an increase in inflammatory pathways). Another ROI DTI study in HIV+ subjects reported a reduction in FA and increased MD, but only in the genu of the corpus callosum (Thurnher et al., 2005). Also, no significant correlation could be demonstrated with the diffusion parameters (FA and MD) and CD4 counts. A more recent study examined differences using a voxel-based analysis to compare HIV+ and control cohorts (Stebbins et al., 2007). There were 30 subjects in each of the groups, and the authors found significant increases in MD for a number of frontal regions. These studies demonstrate that DTI is a sensitive marker for detecting WM abnormalities in HIV and that most of these changes occur in the frontal WM regions.

Most of these DTI studies in HIV^+ patients found decreased FA in the frontal WM regions indicating a loss of white matter integrity even in cognitively asymptomatic subjects. It is not

clear whether or not this is a precursor to the symptoms of apathy. Frontal WM is of particular interest as the fronto-striatal circuits have a role in motivation and goal-driven behaviour (Castellon et al., 2000), and may be involved in the pathology of apathy..

Previous studies have only examined the WM abnormalities found in HIV+ subjects without any other co-morbid conditions such as apathy. Apathy is also prevalent in HIV+ patients, with reported prevalence rates of 30 – 50% in outpatient studies (Castellon et al., 1998; Rabkin et al., 2000). A key study in linking apathy with HIV and fronto-striatal circuits was done by Paul et al., (2005). This work showed a decreased GM volume of the nucleus accumbens, which is central to the goal-directed behaviour pathways in the frontal cortices. It is thus potentially useful to examine WM diffusion to gain a better understanding of the interconnectivity of grey matter regions such as the anterior cingulate and deep gray matter structures. If abnormalities can be demonstrated using DTI in WM tracts connecting frontal WM regions, this could be an early indicator of WM damage in HIV, even before other cognitive impairment is apparent.

3. Study design and methods

3.1 Subject classification

The data that were analysed as part of this thesis were obtained from a larger HIV study, for which recruitment and patient classification was performed by a team of researchers not directly involved with this thesis. For the purpose of this methods section, mention will be made of the subject recruitment and classification protocol to familiarize the reader with the cohort characteristics.

Patients with HIV (n=30) and healthy controls (n=10) were recruited from the Infectious diseases Clinic at Tygerberg Hospital, as well as from the surrounding Cape Town suburbs. Subjects selected for the HIV cohort had to have been on Highly Active Anti-Retroviral Therapy (HAART) for at least 3 months. Subjects were also required to be cognitively normal when screened on the International HIV Dementia Scale (IHDS) scale (IHDS > 10 was required) (Berghuis et al., 1999), with no evidence of substance abuse in the last 6 months. Another exclusion criterion was the presence of any DSM-IV (Diagnostic and Statistical Manual of Mental Disorders 4^{th} edition) disorders and this was determined by a semi-structured Mini International Neuropsychiatric interview (MINI) (Sheehan et al., 1998). The diagnosis of HIV was determined by serological testing with ELISA (enzyme-linked immunosorbent assay) and Western blotting. Ethical approval for the study was obtained from the Committee of Human Research at Stellenbosch University, and informed consent was obtained for all clinical assessments, neuropsychological testing and MRI scans.

The HIV patients were divided into apathetic (n=15) and non-apathetic (n=15) cohorts according to the Apathy Evaluation Scale (AES). This is a clinician administered questionnaire that contains 18 items related to motivation and self-initiation (Marin et al., 1991). These items are rated on a four point Likert scale (1 = no agreement and 4 = full agreement) with subjects specifying the extent to which there is agreement with the statements provided on the self-report. A cutoff score of 38 and above was classified as significant apathy and subjects were divided accordingly. Although the patients displayed no clinical symptoms of major depressive disorder, it was still necessary to distinguish any overlapping symptoms between apathy and depression. Therefore the Hamilton Depression Rating Scale (Hamilton, 1960) was used to examine whether any of the HIV^{+} patients

displayed symptoms of depression. A cutoff score of 16 on the scale was classified as having significant depressive symptoms and therefore was another exclusion criterion for the study.

3.2 Study design

This is the first study examining WM abnormalities in apathetic HIV^+ patients. Previous cerebrovascular infarction case studies have implicated regions such as the internal capsule and genu of the corpus callosum in apathy, and therefore these tracts are of particular interest (Chukwudelunzu et al., 2001; Madureira et al., 1999; Saito et al., 2006). Also, because FA and MD are non-specific markers for demyelination or axonal degeneration, radial and axial diffusivities were examined to determine the physiological factors that are involved in the WM abnormalities. Furthermore, two widely used methods were employed to analyze the DTI data, namely voxel-based comparisons and tract-based spatial statistics. Fiber tracking was performed in the corpus callosum (CC) and anterior thalamic radiation (ATR) to examine whether there would be global changes in FA across the tracts. The results obtained with these methods should provide a complete spectrum of DTI changes across the three cohorts.

Cohorts of normal HIV- subjects, HIV+ non-apathetic patients and HIV+ apathetic patients were studied to examine whether there are abnormal FA, MD, axial and radial diffusivities in apathy-specific cases. For the HIV non-apathetic cohort, similar WM abnormalities are expected than previously demonstrated in the literature, which is changes in frontal WM, internal capsule and corpus callosum. Two different voxel-based techniques are employed to determine if the changes would be consistent across the methods.

The ATR is a tract that is part of the internal capsule and it projects from the thalamus to the prefrontal regions. The corpus callosum is a mass of fibers that are responsible for the interhemispheric connections between corresponding lobes in the brain.

As mentioned above, TBSS, voxel-based analysis and tractography techniques were employed to investigate white matter differences using RD, AD, FA and MD as indices of white matter integrity. These analyses are shown in Fig 3.1., where the following comparisons were made: comparing each individual HIV cohort (n=13) with the healthy controls (n=10), as well as examining differences between the HIV apathetic (n=13) and HIV non-apathetic cohort (n=13). From the original 15 subjects of each HIV cohort 2 were excluded per cohort due to

misregistration and poor scan quality in the voxel-based analysis. In the next sections, these techniques will be explained in more detail.

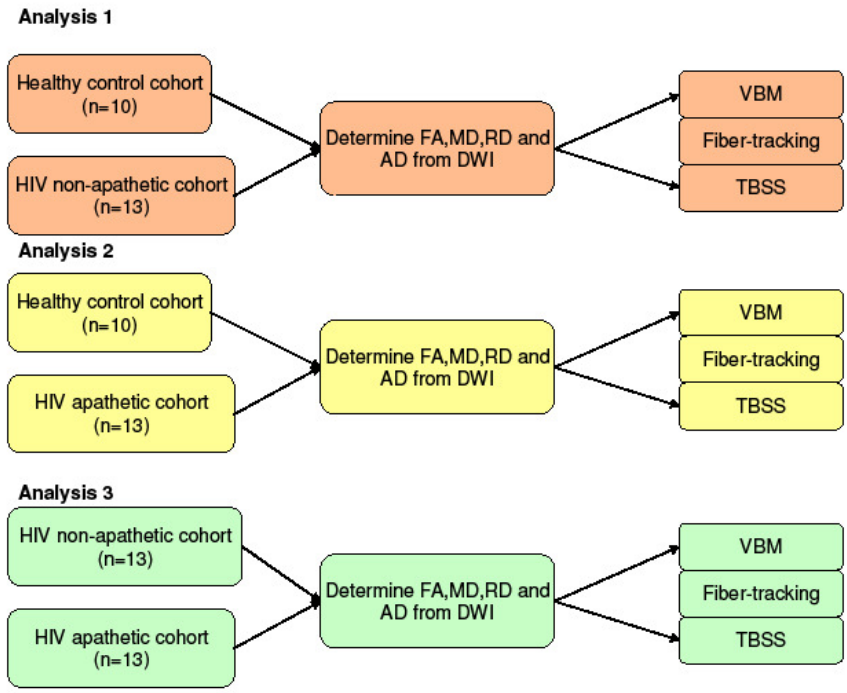

Fig 3.1: Study design. Three separate analyses were performed to examine differences in DTI parameters between the three cohorts. DTI parameters were calculated for each subject with subsequent VBM, fiber tracking and TBSS analysis. Of the 15 subjects in each HIV cohort 2 were excluded per cohort because of misregistration in the voxel-based analysis and poor DTI scan quality. Therefore final numbers were n=13 for the HIV apathetic and non-apathetic cohorts respectively. Abbreviations: **FA**: fractional anisotropy, **MD**: mean diffusivity, **RD**: radial diffusivity, **AD**: axial diffusivity, **DWI**: diffusion-weighted images, **VBM**: voxel-based morphometry, **TBSS**: tract-based spatial statistics

3.3 DTI data acquisition and analysis

The MRI data were acquired on a Siemens Magnetom 3T Allegra scanner at the Cape Universities Brain Imaging Centre (CUBIC). Scans were done within 7 days of screening and neuropsychological testing. The diffusion-weighted images were acquired using the following parameters: 12 diffusion directions, TR=10400 ms, TE=86 ms and a b-value of 1000 sec/mm^2. A single unweighted image (b=0 sec/mm^2) was also obtained. The images were acquired in a 128×128 mm^2 matrix with an in-plane resolution of 1.9 × 1.9 mm^2, 75 slices per direction and a slice thickness of 1.9 mm. This scan sequence was repeated 5 times to increase the signal-to-noise ratio by averaging.

For the purposes of the voxel-based analysis in SPM5 (http://www.fil.ion.ucl.ac.uk/spm), a high-resolution structural T1-weighted magnetization prepared rapid gradient echo (MPRAGE) image was also acquired with the following parameters: TR =2080 ms, TE=4.88 ms and 8º flip angle. The images were acquired in the transverse plane with a 256 x 192 matrix and 176 slices (slice thickness was 1 mm). DTI voxel-based analysis was performed using the SPM5 warping algorithms, and then in-house tools developed at CUBIC using MATLAB. TBSS analysis was performed in FSL (Smith et al. 2006) and subsequent fiber tracking in DTIstudio (Jiang et al., 2006).

Voxel-based DTI analysis

This method is based upon voxel-based morphometry (VBM), which has been broadly applied to examine local grey matter (GM) volume changes between subject groups (Ashburner et al., 2000; Good, 2001). The premise behind the standard VBM method is to align each subject's structural images to a standard space template (such as Talairach (Talairach et al., 1993) or Montreal Neurological Institute (MNI) (http://www.mni.mcgill.ca)) or a study-specific template created from all of the subjects. The alignment is done using an affine registration followed by a non-linear registration (Fig 3.3). After alignment the images can be compared on a voxel-by-voxel basis using statistical parametric mapping. For the purposes of this study, registration was performed in order to align an FA image to a T1 image.

Before continuing with this section, the terms affine and non-linear registration will be introduced as these steps of the process are fundamental to voxel-based analysis and TBSS. The purpose of spatial registrations are to transform the shape, position and/or orientation of an image by manipulating the old coordinates of the brain image to a new coordinate system that brings the image into the same space as the reference image. The transformations are applied in three dimensions and the type of registration can be classified according to the degrees of freedom (DOF). The DOF correspond to the amount of parameters that are varied to transform the target image to align with the reference image.

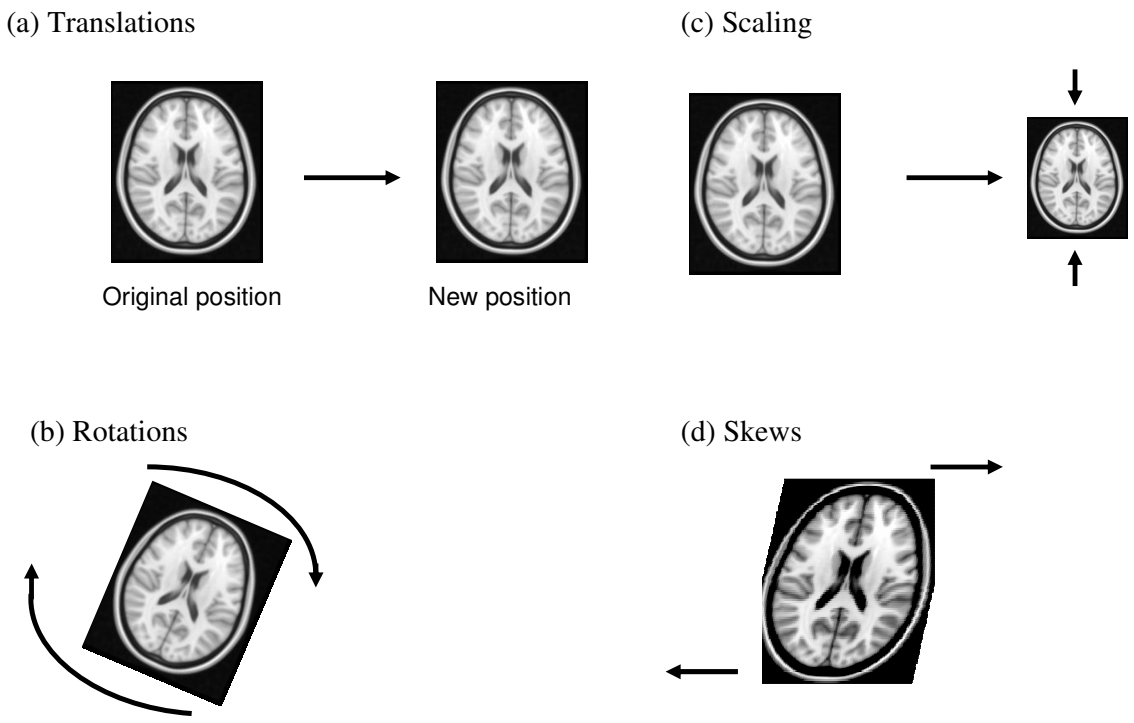

Fig 3.2: Affine transformations (12 degrees-of-freedom (DOF)): This figure demonstrates the 4 types of affine parameters that are applied to a T1 image in this scenario. Each of these parameters can be applied in three orthogonal directions, resulting in a total of 12 parameters or DOF.

Affine registrations can consist of up to 12 DOF. Fig 3.2 shows a representation of the 12 DOF required for an affine registration. These consist of 3 translations, 3 rotations, 3 scalings and 3 skews/shears. This usually provides good initial image alignment. For more subtle changes in alignment, a higher DOF registration needs to be used. This is applied after affine registration to fine-tune the voxel alignment across subjects' brains. This is a slower process than the affine transformations. Mutual information (Papoulis, 1991) is commonly used to specify similar image features between different MRI image contrasts (T1 and FA for example) and even across different imaging modalities (CT and MRI).

For grey matter VBM on high resolution structural images, the registered images are segmented into three tissue classifications, namely GM, WM and CSF (Fig 3.4). Thus only voxels corresponding to a distinct tissue type are compared. The principles of voxel-based analysis can also be applied to diffusion images such as FA and MD maps (Smith et al., 2006). Registration can be performed using the subjects' structural images and/or FA image templates with no segmentation step required.

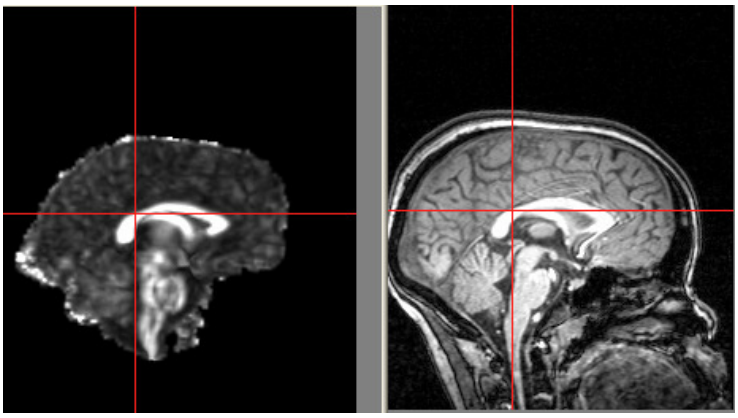

Fig 3.3: Co-registration of an FA image (left) to a T1 structural image (right) using an affine registration followed by non-linear registration. The FA image is aligned with the T1 image despite differences in brain shape and contrast. This is a powerful tool for aligning voxels so that a statistical model can be fitted across many subjects.

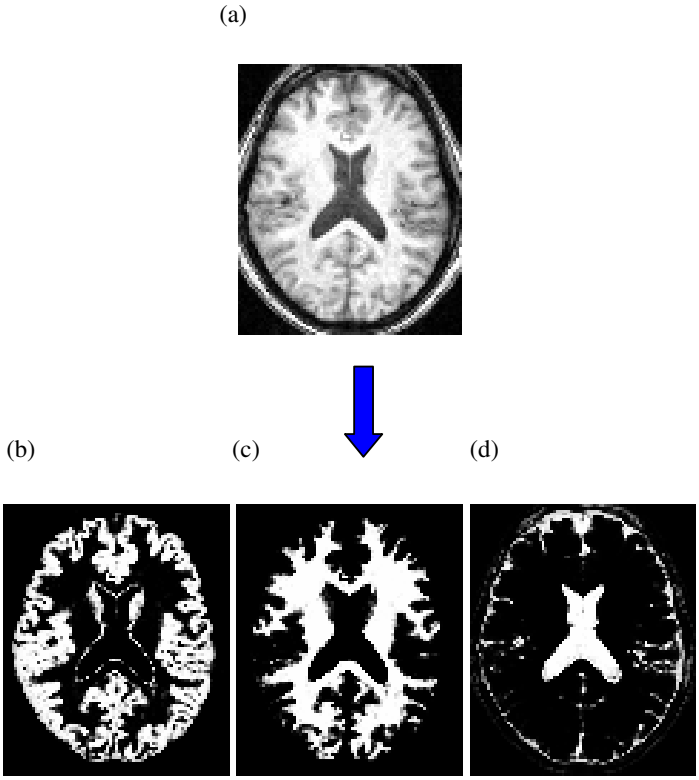

Fig 3.4: Segmentation of a T1 image. In (a) a T1 image of a subject is shown. During VBM analysis a segmentation step is carried out and the brain is classified into 3 groups: (b) grey matter (c) white matter and (d) CSF. This step is necessary for comparing only the grey matter or white matter voxel differences.

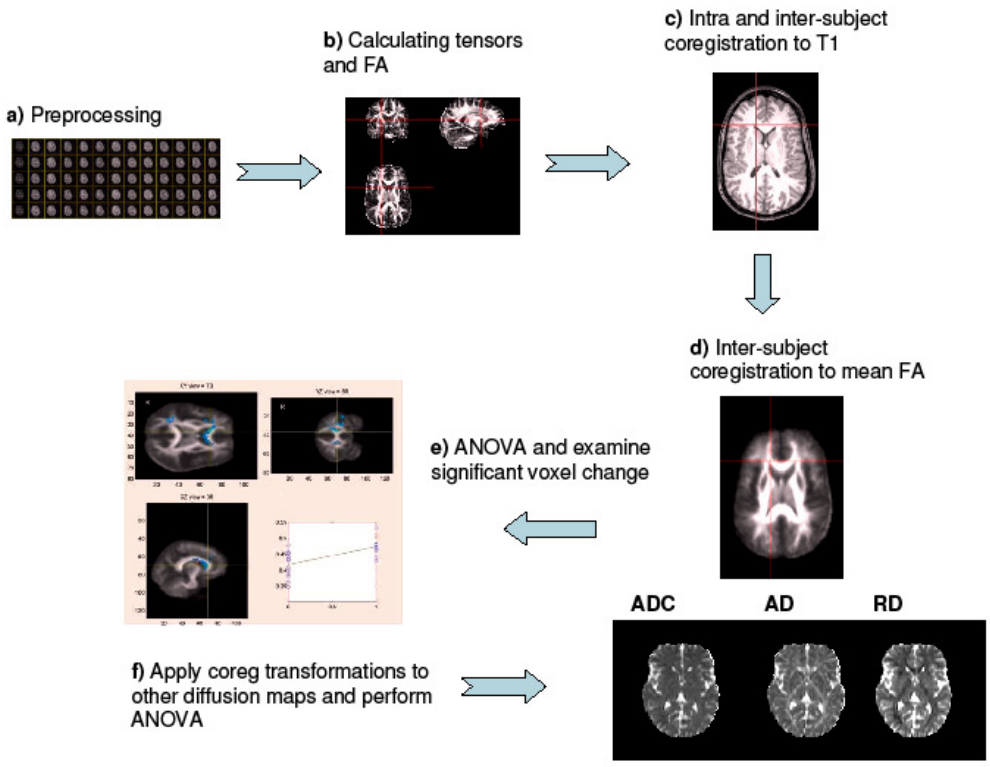

Fig 3.5: Flowchart outlining the methodology of the voxel-based DTI method. Initially (a) preprocessing steps such as brain extraction and eddy current correction are performed. Then the tensors are calculated (b) from the DWI in order to acquire FA images. Intra- and intersubject coregistration steps are then performed (c) to align FA images of all the subjects with a final coregistration to a study-specific FA template (d). An ANOVA statistical model is fitted to each voxel to compare subject cohorts and determine significant local changes in FA (e). The coregistration parameters are then applied to other diffusion maps and ANOVA is performed (f).

Fig 3.5 shows a flowchart of the method employed for this study. These steps are summarised as follows:

(a) Preprocessing. The DWI were exported to FSL 4.1 for eddy current correction, whereby for each of the acquisitions, the diffusion-weighted images were co-registered to the corresponding B0 image. Eddy currents due to the diffusion weighting magnetic field gradients cause distortions in diffusion weighted images which are not present in the B0 images. See Skare et al. (2002) for details on this phenomenon. The corrected diffusion weighted images were exported into Matlab R2007b (Mathworks, Natick, MA) for further processing.

(b) Brain extraction was performed and tensor outliers were rejected as follow: Z-scores were calculated for each data point based on a 25 and 75 percentile limit and data points more than 3 standard deviations away from the mean were then discarded. The DTI data from the five acquisitions were then averaged and tensors were calculated for each voxel. FA, MD, AD and RD were then calculated.
(c) The affine and non-linear registrations were applied to the data in SPM 5 as follows: Firstly within-subject co-registrations were performed by aligning all T1 images. Secondly, an inter-subject co-registration of each subject's transformed FA image (using the transformation parameters as calculated by the intra-subject registration) to a mean T1 template derived from the study cohort. These transformations were then applied to the FA images for each subject.
(d) A mean FA template was created by averaging the coregistered FA images of all subjects and every subject's FA image was co-registered to the mean FA.
(e) An analysis of variance (ANOVA) model was fitted to each voxel to determine whether there are significant changes in FA between groups ($p < 0.05$ uncorrected).
(f) The transformation parameters from each registration step were applied to the MD, AD and RD maps. The ANOVA model was then fitted for statistical comparison using these parameters.

Only significant voxel clusters in WM tracts that were aligned correctly across all the subjects were considered as valid DTI differences. This was achieved by manually inspecting the co-registered FA images for all subjects at any cluster showing up as being significant. Any significant clusters with poorly registered tracts were excluded.

Tract-based spatial statistics

Tract-based spatial statistics (TBSS) was developed by the FMRIB group based at Oxford University (Smith et al., 2006) in order to address some of the shortfalls of a voxel-based DTI analysis. Alignment inaccuracies are minimized by using a mean FA skeleton which represents the centre voxels of major WM tracts (Fig 3.6a).

The TBSS procedure is summarised as follows: The FA images of all subjects are aligned to an FA template image (the FMRIB58 FA target image) using a non-linear registration algorithm. Exact alignment is not necessary at this stage of the processing. After aligning the FA images, a mean FA map is created and the centres of the WM tracts are determined by a process known as "skeletonisation" of the mean FA map. The voxel with the highest FA is

identified as the tract centre after searching locally in a direction perpendicular to the tract. A threshold FA value of 0.2 is usually enforced to exclude any regions with low FA or high inter-subject variability (for example the parts of the WM tracts that run to the outer edges of the cortex). For the next step each subjects' registered FA image is projected onto the mean FA map skeleton. This process entails looping through all points on the mean skeleton image and conducting a search perpendicular to the tract to find the corresponding maximum FA value on each subject's registered FA image. These maximum FA values are then assigned to the corresponding skeleton voxel for each individual image (Fig 3.6b). This perpendicular search is limited by constraining the search to areas close to the skeleton. For this purpose a skeleton distance map is created to encode each brain voxel with a distance value for the nearest skeleton point. Fig 3.6 shows an example of such a distance map with a colour overlay indicating the distance value. A search is performed from a skeleton point while the intensity value is increasing and as soon as there is a decreased intensity value, the search will terminate. Therefore no two voxels will be projected onto the same point of the skeleton. As soon as the voxel with the maximum FA value is found for each search it will be extracted and placed into the subject's FA skeleton. Finally a general linear model is applied to compare each skeleton voxel independently between subject cohorts. To correct for multiple comparisons a permutation-based approach is used, in other words, the t-value of the independent sample t-test is compared to a null distribution of maximum t-values.

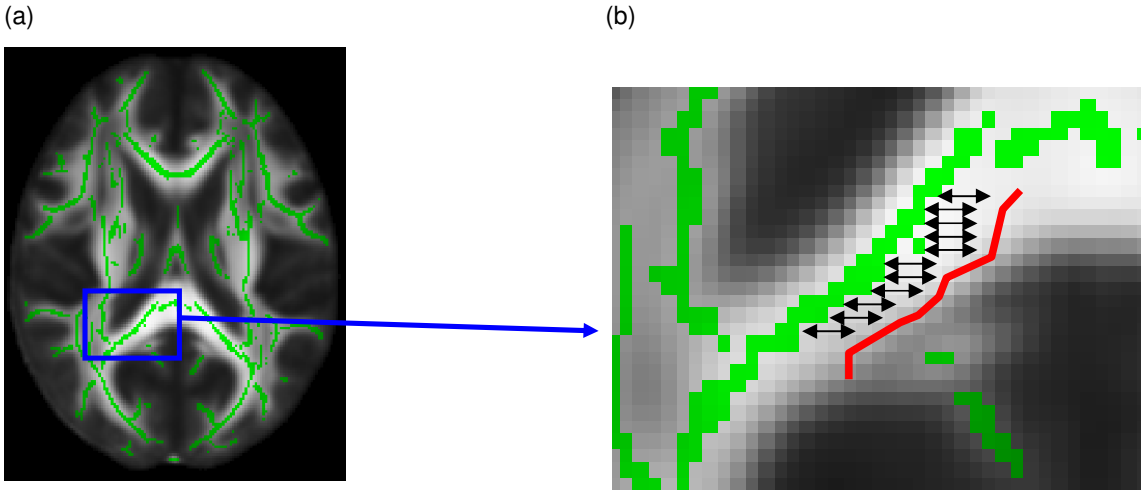

Fig 3.6: A mean FA skeleton of an FA template. (a) The voxel-based analysis is restricted to the centre of the WM tract bundles as represented by the green "skeleton" of the tracts. This has the benefit that partial volumes of the GM and CSF do not influence the results. (b) During the skeleton projection phase, each subject's WM voxel with the maximum FA for a perpendicular region is shifted to align with the mean FA skeleton. Using the splenium region here as an example, the voxel with the highest FA value is searched in each perpendicular direction as represented by the black arrows. The red line represents the maximum FA values for the WM tract of a subject that is being projected to the mean FA skeleton.

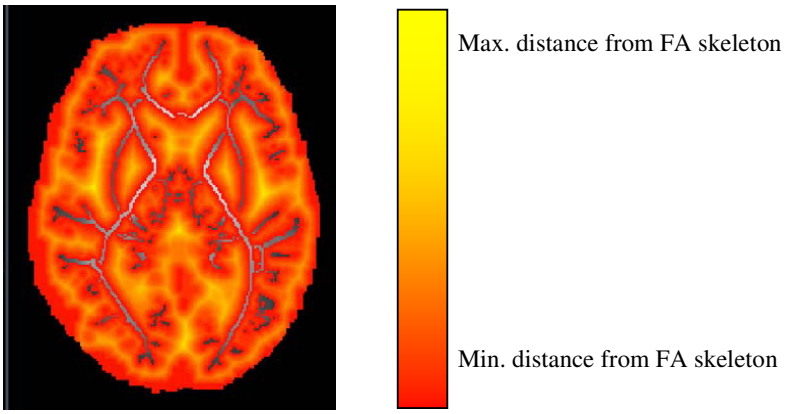

Fig 3.7: An example of a skeleton distance map. Each brain voxel is encoded with a value indicating the distance from the nearest skeleton voxel. Therefore no two voxels will be projected onto the same point of a FA skeleton. The skeleton voxels display as grey, because the distance value is zero.

TBSS application to this study

Fig 3.8 shows a flow-chart outlining the TBSS protocol that has been applied in this study:

(a) The preprocessing was identical to Steps (a) and (b) on page 23. The subsequent analysis was performed in the FSL 4.1 software package.
(b) Every subject's FA image was aligned to a target FMRIB FA template.
(c) All images are subsequently registered to a MNI152 T1 template.
(d) A mean FA image was created using all the subjects' FA maps.
(e) Every subject's FA image was projected onto the mean skeleton for alignment of the tract centre voxels by utilising a distance map to calculate voxels representing the WM centres.
(f) After the projection step, a general linear model (GLM) was fitted for statistical analysis of each skeleton voxel with subsequent permutation-based correction for multiple comparisons at $p < 0.05$. This process was repeated for the other diffusion maps as well, with skeletonisation and projection steps occurring in the space of the mean FA skeleton.

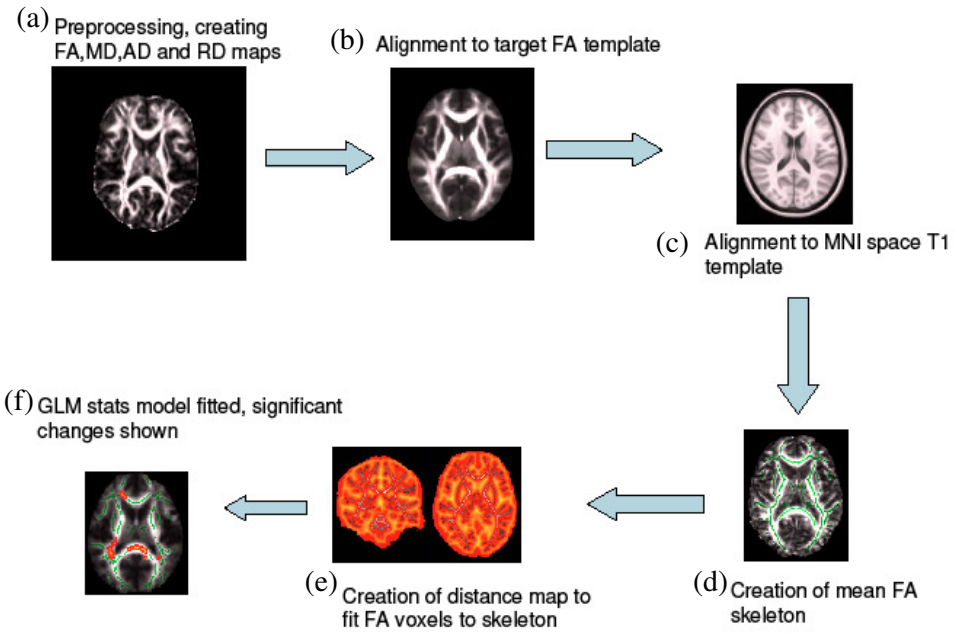

Fig 3.8: Flowchart outlining the steps for TBSS analysis. After preprocessing the FA, MD, AD, and RD maps were created (a). These images were coregistered to a target FA template and an MNI152 T1 template respectively (b-c). After registration the images were resliced and a mean FA skeleton was created (d). Distance maps were created for the purpose of projecting individual FA images to the mean skeleton (e). After projection, a GLM model was fitted to each skeleton voxel to examine WM differences (f). The statistical threshold was $p < 0.05$ corrected for multiple comparisons. These steps were repeated for MD, AD and RD.

DTI tractography

DTI has been shown to provide information about the extent of diffusion anisotropy in brain tissue, but the orientation of this anisotropy is also useful. The principal axis of the tensor in a white matter voxel is assumed to describe the dominant fiber orientation in that voxel. From this assumption, 2D and 3D vector fields can be obtained that are a representative of fiber orientation for each voxel in a diffusion-weighted image (Basser et al., 2002). DTI fiber tracking (or tractography) is a method in which WM fibers can be reconstructed and visualized using the information contained in a tensor field (Fig 3.9). A commonly used technique involves selecting a starting seed, and using simple line propagation in the principle eigenvector field to follow the WM tract of interest. While following the principle eigenvector direction, the tract will encounter the boundary of the next voxel and the direction of tracking is changed to the new voxel's direction (Jiang et al., 2006). The propagation ends when a

region with low anisotropy is reached or when the tract angle between two iterations is greater than a specified threshold. Parameters such as the mean FA and MD for the tract of interest can be extracted from these reconstructed fibers and used for statistical analysis.

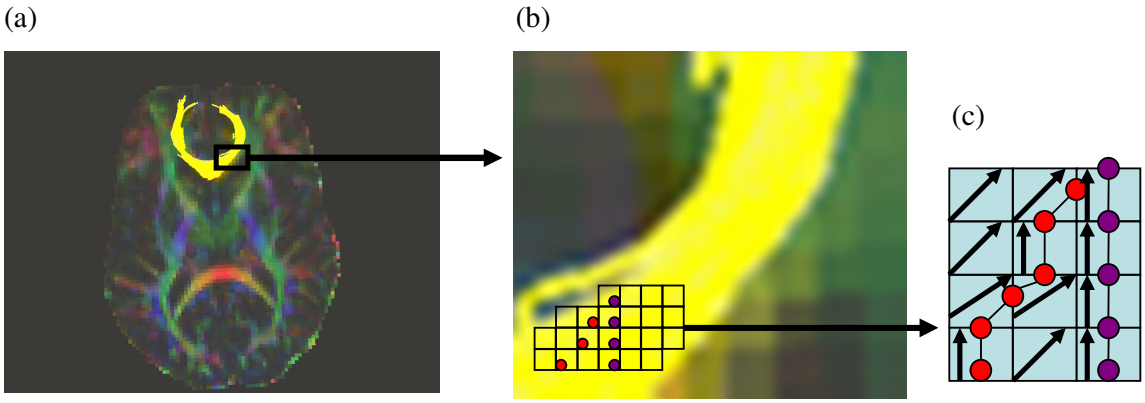

Fig 3.9: Simple tractography algorithm. An example of a tract is shown, namely the genu of the corpus callosum (a). The largest eigenvector direction (or principle diffusion direction) is used for the fiber tracking (the colour map corresponds to the largest eigenvector direction where red is left-right, green is anterior-posterior, and red is cranio-caudal). (b) Region of interest. (c) Magnified region showing the tracking initiated from two seed points (the red and purple dots at the bottom of the image). When following along the eigenvector, the tracking will change direction every time the edge of a neighbouring voxel is reached. This process is repeated several times to obtain a fiber trajectory

Targeting specific tracts using Fiber Assignment by Continuous Tracking (FACT)

Fiber tracking was used to examine two tracts of interest: the anterior thalamic radiation (ATR) (Fig 3.10a) and the corpus callosum (Fig 3.10b) for the healthy control cohort, HIV apathetic cohort and the HIV non-apathetic cohort. The ATR tracking was performed in DTIstudio (Jiang et al., 2006) using the Fiber Assignment by Continuous Tracking (FACT) approach (Mori et al., 1999; Xue et al., 1999). To identify tracts of interest, tracking is performed from every voxel in the whole dataset and trajectories passing through user-defined regions of interest are identified. This method of tracking from each voxel in the image is known as brute force fiber tracking (Conturo et al., 1999; Stieltjes et al., 2001; Werring et al., 2000).

In order to define WM tracts of interest, a region of interest (ROI) needs to be introduced to demarcate known fiber bundles. For this purpose multiple ROI's with Boolean operations enable a user to select specific tracts. Three common 3 operations are AND (specify tracts that are passing through both ROI's), OR (specify tracts that are independent of one another, but both required) and NOT (excluding tracts) (Conturo et al., 1999; Catani et al., 2002). An

example of this is shown in Fig 3.11: If ROI-1 was selected first and ROI-2 second, then the AND operation will restrict the selection to the fibers to those passing through both of the ROI's, and the OR operation will select fibers going through ROI-1 and ROI-2 independently. If the NOT operation was applied to ROI-2, then any fibers passing through this region will be excluded. In this manner, specific regions in WM tracts can be selected.

(a) Anterior thalamic radiation (b) Corpus callosum

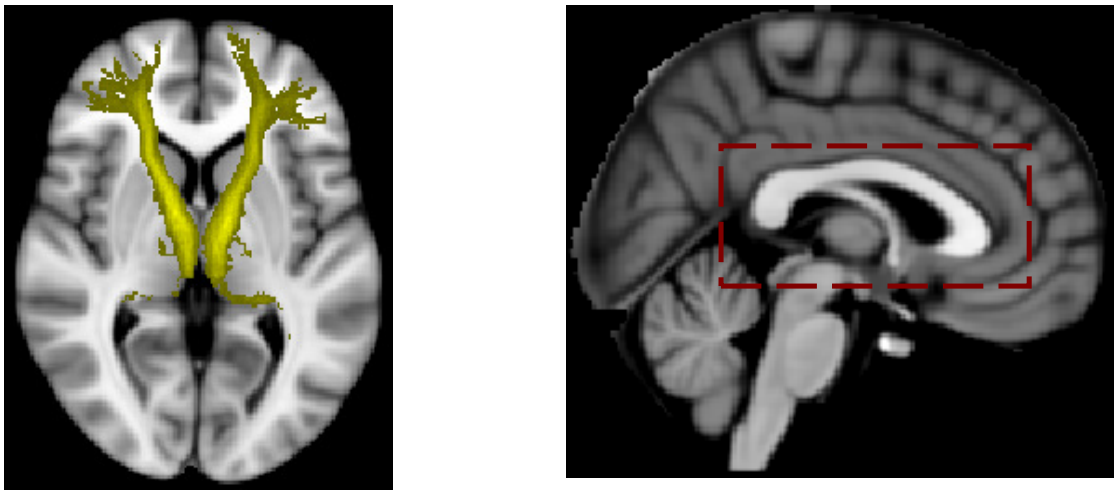

Fig 3.10: A representation of the anterior thalamic radiation (ATR) and corpus callosum (CC). (a) The ATR projects from the thalamus into the prefrontal cortex and is part of the anterior limb of the internal capsule. (b) The corpus callosum is a large body of WM fibers that is responsible for inter-hemispheric communication between lobes.

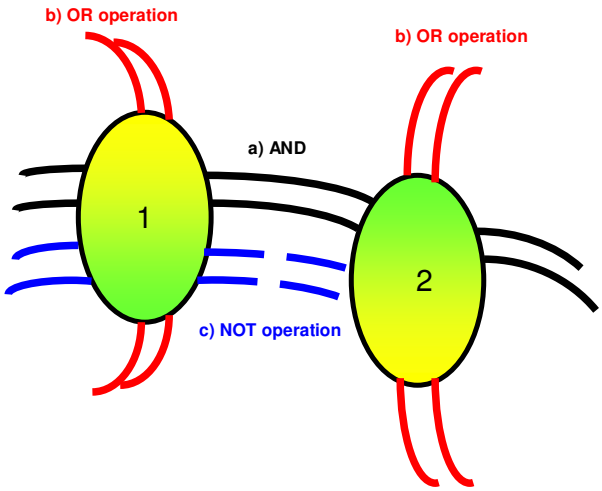

Fig 3.11 An illustration of the Boolean operators used in tractography. Regions of interest (ROI's) are selected by the operator. For the AND operation (a): if ROI-1 was selected first and ROI-2 second, then any fibers intersecting both the ROI's will be reconstructed. Fibers that pass through only one ROI are ignored. For the OR operation (b): any fibers passing through ROI-1 or ROI-2 are reconstructed, and fibers passing through both will be ignored. For the NOT operation (c): if ROI-2 was selected with the NOT parameter then only fibers passing through ROI-1 are reconstructed.

Tracking the anterior thalamic radiation

For the purposes of tracking the ATR (Fig 3.10a) preprocessing steps were applied as described for the voxel-based analysis (eddy current correction, outlier rejection and averaging). The data were then imported into DTIstudio for further analysis. Eigenvalues and eigenvectors were calculated from the DTI tensors and from this the fractional anisotropy (FA) map was created. A colour map of the principal eigenvector (such as shown in Fig 3.9) was used to define ROI's for fiber tracking. The ATR was reconstructed according to a protocol that has been tested for inter and intra-rater variability (Wakana et al., 2007). The FACT method was applied as previously explained, with an FA threshold of 0.2 and an angle threshold of 0.75 radians as tractography termination criteria. The multi-ROI approach was performed with Boolean operators and careful scrutiny of the anatomy using a DTI white matter atlas (REF). The same reconstruction protocol was applied for each subject. The exact operations are described as follows (refer to Fig 3.12): A coronal slice was selected in the middle of the corpus callosum, with the first ROI drawn around the anterior limb of the internal capsule. With the AND operation a second ROI was drawn at the anterior edge of the pons in the coronal view. The entire thalamus was selected for the second ROI. Any trajectories crossing the corpus callosum to enter the contralateral hemisphere, and fibers projecting to the prefrontal cortex, were excluded using the NOT operator. Mean FA and MD values for the ATR were calculated and exported to SPSS 16.0 for statistical analysis. Differences in FA and MD were examined by applying an independent sample t-test at $p < 0.05$.

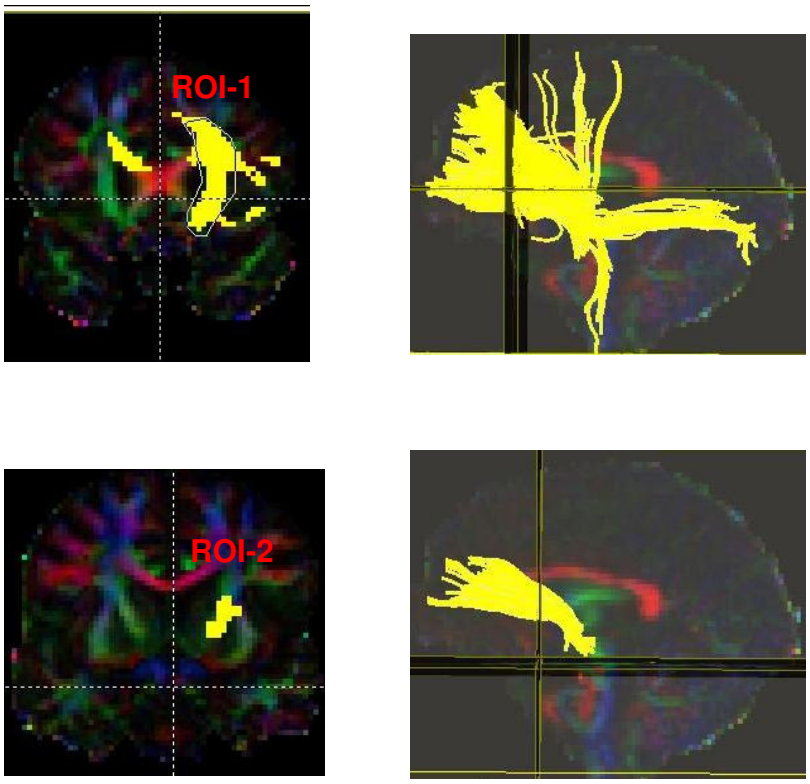

Fig 3.12 ROI's for tracking the ATR. The ATR was reconstructed by following a protocol designed by Wakana et al. (2007) for DTIstudio. A coronal slice is selected at the genu of the corpus callosum for the first ROI. For the second ROI, a coronal slice is selected at the anterior region of the pons and the thalamus was outlined with the AND operation. Thus, only fibers passing through ROI-1 and ROI-2 are reconstructed. Any fibers that cross into the contralateral hemisphere of the corpus callosum and any fibers that don't project to the prefrontal cortex were excluded using the NOT operation.

Tracking the corpus callosum

Preprocessing steps were implemented as describe above for the ATR. An ROI was drawn around the entire corpus callosum in the mid-sagittal view. Further ROI's were defined for 5 functional regions in the corpus callosum (Fig 3.13).These segments were originally defined by Witelson (1989) and later redefined by Hofer et al. (2006). This entails dividing the CC into the anterior third (fibers that project into the prefrontal, premotor and supplementary regions), the anterior midbody (fibers projecting into the motor cortex), the posterior midbody (fibers projecting into the somaesthetic and posterior parietal regions), the isthmus (fibers projecting into the posterior parietal and superior temporal regions) and the splenium (fibers projecting into occipital and inferior temporal regions). These functional regions were reconstructed by tractography. Any fibers that were not part of the corpus callosum were excluded with the NOT operator. Only FA values for the functional regions (left and right

hemisphere respectively) were exported to SPSS 16.0 for statistical analysis. Differences in FA were examined by applying an independent sample t-test at $p < 0.05$.

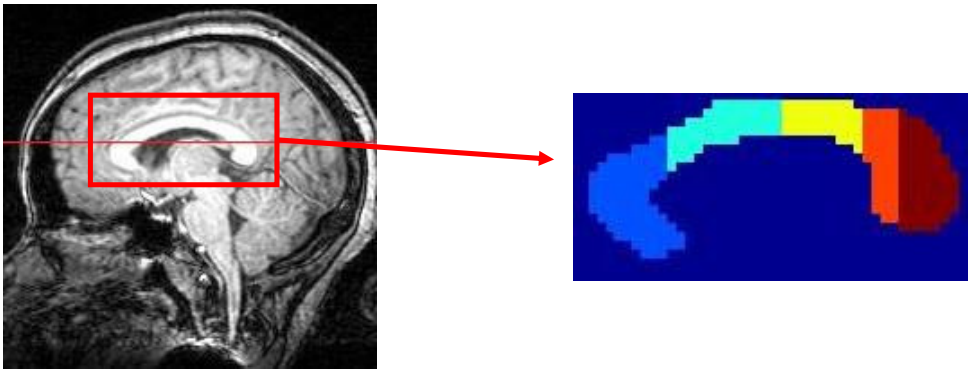

Fig 3.13 The functional regions of the CC. Hofer (2006) divided the corpus callosum into 5 regions corresponding with the respective hemispheres. The regions are the anterior third (blue), anterior midbody (green), posterior midbody (yellow), isthmus (orange) and splenium (red). Each of these corresponds to a functional brain region in both hemispheres.

4. Results

The following sections present the results obtained for the voxel-based, TBSS and tractography analyses. Firstly, the TBSS and voxel-based results for the comparison between the healthy control cohort and the HIV non-apathetic cohort will be presented to show the effects of only the virus on the DTI metrics. This will be followed by the findings for the comparison between the healthy control cohort and the HIV apathetic cohort to demonstrate the added effects of apathy on the DTI data. Finally, the findings from the comparison between the two HIV groups will be presented to demonstrate the effect of apathy within HIV patients. The tractography analysis for the anterior thalamic radiation and the corpus callosum did not show any differences at a significance threshold of p=0.05 and the data are presented as an Addendum. Table 4.1 at the end of this Chapter provides a summary of the results as obtained with TBSS and voxel-based analysis.

4.1 Comparison of the HIV non-apathetic cohort with the healthy control cohort

Fig 4.1. presents the results from the voxel based analysis and Fig 4.2. presents the results from the TBSS analysis. All changes noted are for the HIV non-apathetic cohort relative to the healthy control cohort.

Changes in FA and MD

For the voxel based analysis:

- Decreased FA in the right anterior corona radiata.
- Increased FA in the left sagittal stratum (which is composed of the inferior longitudinal fasciculus and fronto-occipital fasciculus).
- Decreased MD in the left sagittal stratum.

No changes in FA were detected with the TBSS analysis.

Changes in AD and RD

For the voxel based analysis:

- The only change in AD was a decrease in the left sagittal stratum.
- Decreased RD was detected in the left sagittal stratum and increased RD in the right anterior corona radiata.

However, there were more differences that were significant in the TBSS output: Decreased AD was found for the left anterior limb of the internal capsule, the cerebral peduncles (bilaterally), the left middle cerebellar peduncle, the superior cerebellar peduncles (bilaterally) and the posterior limb of the internal capsule (bilaterally).

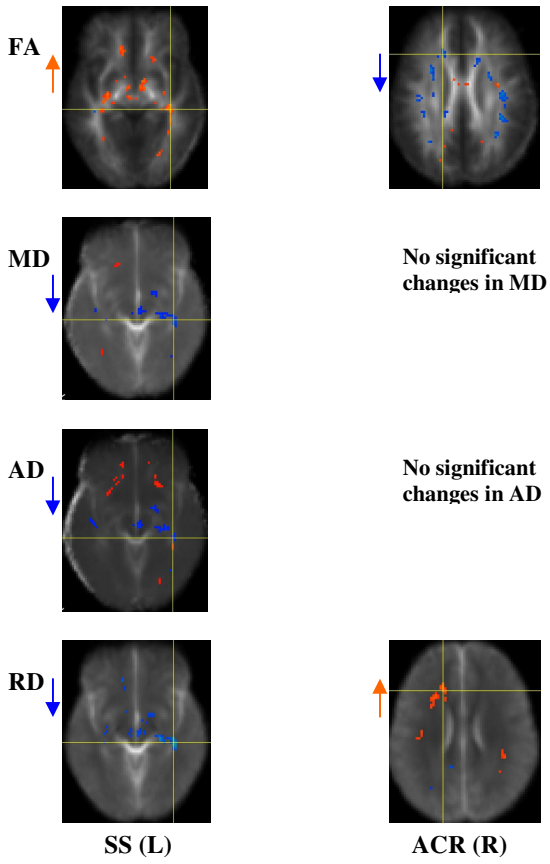

Fig 4.1: Voxel-based DTI analysis for healthy controls vs HIV non-apathetic cohort as performed in MATLAB. Shown here are the changes in diffusivities for the HIV non-apathetic cohort (n=13) when compared to a normal healthy control cohort (n=10). A general linear model was applied to examine statistical significance at $p < 0.05$ uncorrected threshold. (Abbreviations: **SS** - Sagittal stratum; **ACR** - Anterior corona radiata)

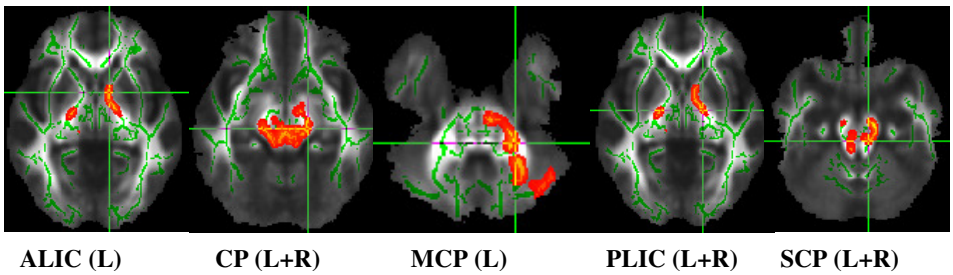

Fig 4.2: TBSS DTI results showing decreased AD in the HIV non-apathetic cohort (n=13) when compared to a healthy control cohort (n=10). (Abbreviations: **ALIC** - Anterior limb of the internal capsule; **CP** - Cerebral peduncle; **MCP** - Middle cerebellar peduncle; **PLIC** - Posterior limb of the internal capsule; **SCP** - Superior cerebellar peduncle). Permutation-based statistics was performed for $p < 0.05$ family-wise error corrected.

4.2 Comparison of the HIV apathetic cohort with the healthy control cohort

Fig 4.3 presents the results from the voxel based analysis and Figs 4.4 – 4.6 present the results from the TBSS analysis. All changes noted are for the HIV apathetic cohort relative to the healthy control cohort.

Changes in FA and MD

For the voxel-based analysis:

- Decreased FA in the left posterior and anterior corona radiata.
- Increased MD in the left posterior corona radiata.

For the TBSS analysis:

- Decreased FA in the bilateral genu, body and splenium of the corpus callosum.
- Decreased FA in bilateral regions of the posterior and anterior corona radiata.
- Bilateral decreases in FA for the cingulum.
- Bilateral decreases in FA for the superior corona radiata.
- No changes in MD were found.

Changes in AD and RD

For the voxel-based analysis:

- Decreased AD in the left posterior corona radiata.
- Decreased AD in the right corticospinal tract.
- Increased RD in the corticospinal tracts bilaterally.
- Increased RD in the posterior corona radiata bilaterally.

For the TBSS analysis:

- Decreased AD in the bilateral regions of the anterior limb of the internal capsule and the left posterior limb.
- Decreased AD in the bilateral cerebral peduncles.
- Decreased AD in the bilateral corticospinal tract.
- Decreased AD in the left external capsule.
- Decreased AD in the CC genu, body and splenium.
- Decreased AD in the middle and superior cerebellar peduncles.
- Decreased AD in the left superior longitudinal fasciculus.
- Increased RD in the left anterior and superior corona radiata.

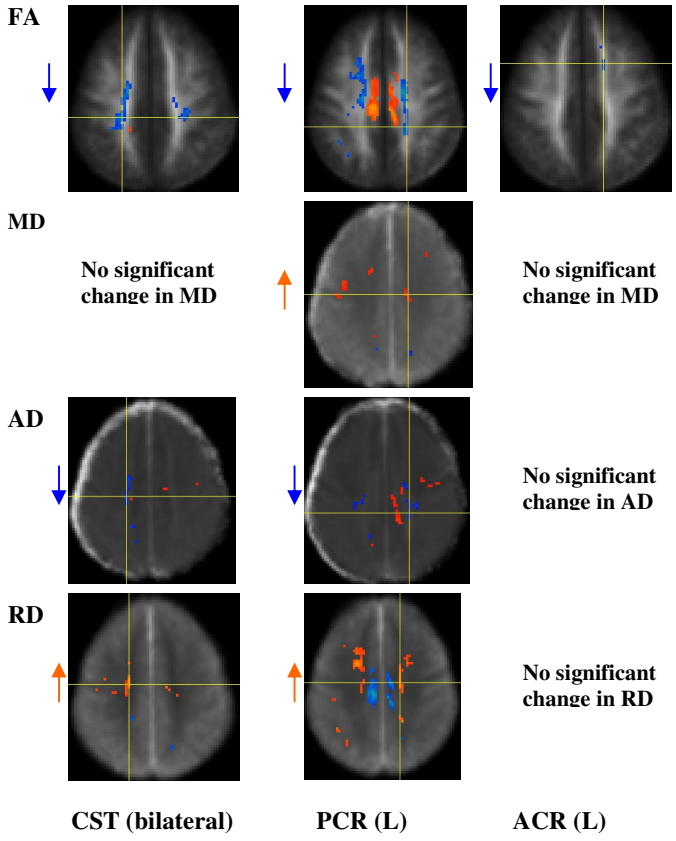

Fig 4.3: Voxel-based DTI analysis for healthy controls vs HIV apathetic cohort as performed in MATLAB. Changes in DTI metrics for the HIV apathetic cohort (n=13) when compared to a normal healthy cohort (n=10). A general linear model was applied to examine statistical significance at $p < 0.05$ uncorrected threshold. (Abbreviations: **CST** - Corticospinal tract; **CC** - Corpus callosum; **PCR** - Posterior corona radiata; **ACR** - Anterior corona radiata)

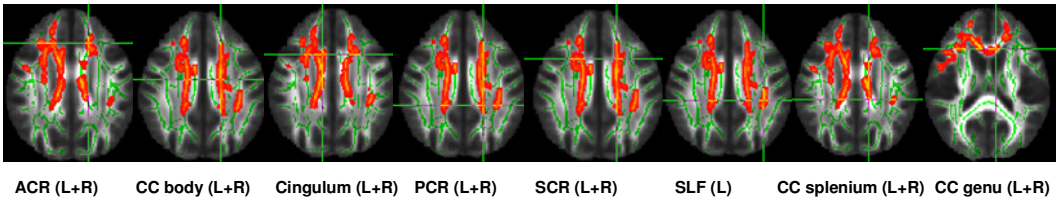

Fig 4.4: TBSS DTI results showing decreased FA in the HIV apathetic cohort (n=13) when compared to the healthy control cohort (n=10). (Abbreviations: **ACR** - Anterior corona radiata; **CC** - Corpus callosum; **PCR** - Posterior corona radiata; **SCR** - Superior corona radiata; **SLF** - Superior longitudinal fasciculus). Permutation-based statistics was performed for $p < 0.05$ family-wise error corrected.

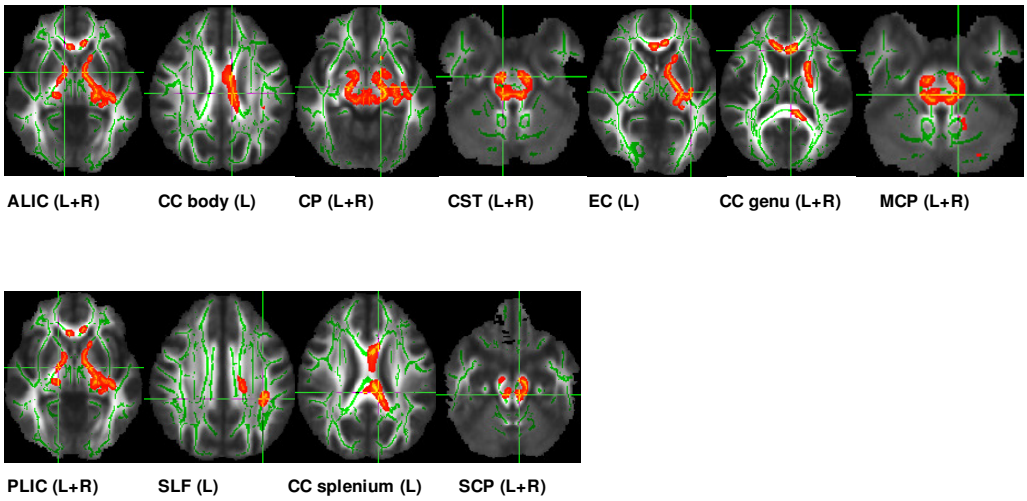

Fig 4.5: TBSS DTI results showing decreased AD in the HIV apathetic cohort (n=13) when compared to a healthy control cohort (n=10). (Abbreviations: **ALIC** - Anterior limb of the internal capsule; **CC** - Corpus callosum; **CP** - Cerebral peduncle; **CST** - Corticospinal tract; **EC** - External capsule; **MCP** - Middle cerebellar peduncle; **PLIC** - Posterior limb of the internal capsule; **SLF** - Superior longitudinal fasciculus; **SCP** - Superior cerebellar peduncle). Permutation-based statistics was performed for $p < 0.05$ family-wise error corrected.

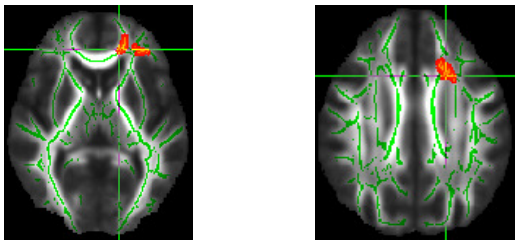

Fig 4.6: TBSS DTI results showing increased RD in the HIV apathetic cohort (n=13) when compared to a healthy control cohort (n=10). (Abbreviations: **ACR** - Anterior corona radiata; **SCR** - Superior corona radiata). Permutation-based statistics was performed for $p < 0.05$ family-wise error corrected.

4.3 Comparison of the HIV non-apathetic cohort compared to the HIV apathetic cohort

Fig 4.7 presents the results from the voxel based analysis. No significant changes were noted in the TBSS analysis for any of the DTI metrics. All changes noted are for the HIV apathetic cohort relative to the HIV non-apathetic cohort.

Changes in FA and MD

For the voxel-based analysis:

- Decreased FA in the bilateral regions of the CC genu and the left CC body region.
- Decreased FA in the right anterior thalamic radiation.
- Decreased FA in the right superior corona radiata.
- Increased FA in the CC splenium region.
- Decreased MD in the CC splenium region.
- Increased MD in the CC genu region.
- Increased MD in the right superior corona radiata.

No changes were found for the TBSS analysis.

Changes in AD and RD

For the voxel-based analysis:

- Increased AD in the left hemisphere of the CC splenium.
- Increased AD in the right superior corona radiata.
- Decreased RD in the left hemisphere of the CC splenium.
- Increased RD in the bilateral regions of the CC genu.

No changes were found for the TBSS analysis.

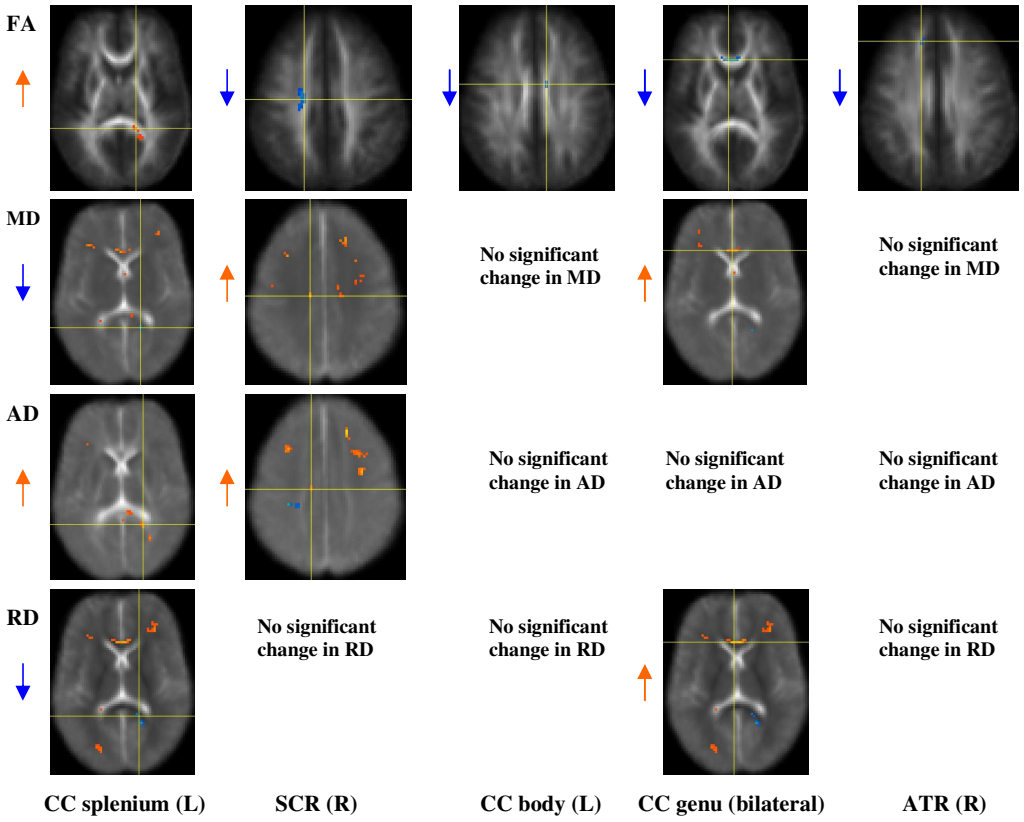

Fig 4.7: Voxel-based DTI analysis for HIV apathetic vs HIV non-apathetic cohorts as performed in MATLAB Changes in DTI metrics for the HIV apathetic cohort (n=13) when compared to the HIV non-apathetic cohort (n=13). A general linear model was applied to examine statistical significance at a $p < 0.05$ uncorrected threshold. (Abbreviations: **CC** - Corpus callosum; **SCR** - Superior corona radiata; **ATR** – Anterior thalamic radiation)

Table 4.1: Summary of voxel-based and TBSS results for the 3 group comparisons. Refer to Fig 4.1 – 4.7 for the anatomical regions and abbreviations. The statistical threshold was $p < 0.05$ corrected for multiple comparisons for the TBSS analysis and $p < 0.05$ uncorrected for the voxel-based analysis. (Abbreviations: **ATR** – Anterior thalamic radiation; **SCR** – Superior corona radiate; **CC** – Corpus callosum; **CST** – Corticospinal tract; **ACR** – Anterior corona radiate; **PCR** – Posterior corona radiate; **SS** – Sagittal stratum; **ALIC** – Anterior limb of internal capsule; **CP** – Cerebral peduncle; **EC** – External capsule; **MCP** – Middle cerebellar peduncle; **PLIC** – Posterior limb of internal capsule; **SLF** – Superior longitudinal fasciculus; **SCP** – Superior cerebellar peduncle)

Analysis	**FA changes**	**MD changes**	**AD changes**	**RD changes**
HIV non-apathetic (n=13) vs HIV apathetic (n=13) (*changes noted only in VB analysis*)	Decreases: ATR (R) SCR (R) CC genu (L+R) CC body (L) Increases: CC splenium (L)	Increases: SCR (R) CC genu (L+R) Decreases: CC splenium (L)	Increases: SCR (R) Decreases: CC splenium (L)	Increases: CC genu (L+R) Decreases: CC splenium (L)
Healthy control (n=10) vs HIV apathetic (n=13) (*changes in TBSS and VB*)	Decreases: *For VB:* CST (L+R) *For TBSS:* CC body (L+R) Cingulum (L+R) SCR (L+R) *For VB+TBSS* ACR (L+R) PCR (L+R) CC genu (L+R) CC splenium (L+R)	Increases: *For VB:* CC genu (L+R) PCR (L)	Decreases: *For VB:* PCR (L) *For TBSS:* ALIC (L+R) CC body (L) CP (L+R) EC (L) CC genu (L+R) MCP (L+R) PLIC (L+R) SLF (L) CC splenium (L) SCP (L+R) *For VB+TBSS* CST (L+R)	Increases: *For VB:* CST (L+R) CC genu (L+R) CC splenium (L+R) PCR (L) *For TBSS:* ACR (L+R) SCR (L+R)
Healthy control (n=10) vs HIV non-apathetic (n=13) *(changes in TBSS and VB for AD)*	Decreases: *For VB:* ACR (R) Increases: *For VB:* SS (L)	Decreases: *For VB:* SS (L)	Decreases: *For VB:* SS (L) *For TBSS:* ALIC (L) CP (L+R) MCP (L) SCP (L+R) PLIC (L+R)	Decreases: *For VB:* SS (L) Increases: *For VB:* ACR (R)

5. Discussion

The aim of this study was to examine white matter changes in an HIV non-apathetic and HIV apathetic population when compared to each other and a matched healthy control cohort. This was accomplished by comparing DTI parameters across the three groups with two voxel-based methods and fiber tractography. Abnormalities in FA were detected between all three groups. To delineate the underlying physiological influences on white matter, the mean, axial and radial diffusivities were also compared with TBSS and voxel-based techniques. Decreased AD corresponds to axonal damage, with increased RD and unchanged AD corresponding to demyelination (Song et al., 2002; Song et al., 2005). MD is an average of the major diffusion directions and increases in this diffusivity indicates increases in extracellular fluid which could be due to inflammatory processes (Assaf et al., 2007).

5.1 Fractional anisotropy and mean diffusivity changes in HIV patients with and without apathy

This section discusses the changes noted between the HIV non-apathetic and apathetic patients and the normal controls. Refer to Table 5.1 for a summary of these changes and the relation with previous DTI work in HIV patients. Many of the WM differences between controls and HIV patients identified in this study correspond to previous studies. However, making direct comparisons with previous data is complicated by the inconsistent results of previous studies, differences in the study population demographics, study designs and methods of DTI analysis. A study by Pomara et al (2001) used a ROI based approach and found FA abnormalities in frontal WM regions as well as the posterior limbs of the internal capsule. However in contrast to this study, Pomara et al. found no statistically significant changes in MD. Thurnher et al. (2005) also showed a decreased FA in the genu of the corpus callosum in HIV patients compared to healthy controls. However, a ROI study by Wu et al. (2006) showed significant decreases in FA only in the splenium and not the genu and frontal WM regions (with increased MD in the splenium as well). For this study, prominent FA decreases in the CC have been found for the HIV apathetic cohort, with changes located in the genu, body and splenium regions. However, for this study MD decreases were noted in the splenium with increased MD in the genu. Although Wu et al. did not find any significant decrease in genu FA, there was a correlation with visuoconstruction and visual memory deficits. This indicates that FA changes in the genu of the CC can influence cognitive function

of frontal regions, and could be possible early markers for HIV-associated cognitive impairment. For the tractography analysis in the CC, no significant changes were demonstrated at $p < 0.05$. However, there was a trend of decreased FA in the CC fibers connecting prefrontal regions (located in the genu) and CC fibers connecting primary sensory regions (located anterior to the splenium) in the HIV cohorts compared to healthy controls (Table A2 in the Addendum A).

For the internal capsule, previous groups have demonstrated increased FA in the posterior limb in HIV patients (Pomara et al., 2001) and no MD changes in this region for HIV-demented individuals (Chen et al., 2009). In contrast, no changes in FA was noted in the internal capsule for both the HIV non-apathetic and apathetic groups in this study, which could indicate that dysfunction in the internal capsule is not specific to HIV-associated apathy.

Another WM structure that exhibited changes in both the HIV apathetic and non-apathetic groups was the corona radiata. FA decreases in the anterior region were found for this structure in both the TBSS and voxel-based analysis, as well as increases in MD for the posterior and superior regions. Similar results were reported by Chen et al. (2009). A related study by Ragin et al. (2005) demonstrated that MD values of the corona radiata in HIV patients were significantly correlated with poor performance on visual memory and visuoconstruction tasks, indicating a role for this structure in HIV associated cognitive impairment. A region identified by this study, which has not been demonstrated in previous HIV studies, is the sagittal stratum where increased FA and decreased MD were noted. This was an interesting finding because it is specific to the HIV non-apathetic cohort. The sagittal stratum is a region that consists of the inferior longitudinal fasciculus and inferior fronto-occipital fasciculus (Aralasmak et al., 2006). These tracts are important in the emotion that presents with visual stimuli. Studies in patients with major depression have shown that there are alterations in the emotional perception of visual input (Phillips et al., 2003). The reason that this result was not present in HIV patients with apathy remains unclear. Additional regions not reported previously are in the frontal WM, where decreases in FA are demonstrated for the HIV apathetic cohort, specifically in the cingulum and anterior thalamic radiation. This was specific to the apathetic cohort only (compared to the non-apathetic HIV cohort), and indicates changes in the anterior cingulate frontal-subcortical circuit, a region previously implicated in apathy associated with various pathologies (Levy et al., 2006).

Table 5.1. Summary of the regions with FA and MD abnormalities in the three cohorts and the comparisons and differences with previous DTI work in HIV. The changes in FA and MD mentioned here are in comparison with healthy controls for all studies.

Regions with abnormal white matter in HIV patients	**Similiarities with other studies**	**Studies with different results**	**Analysis methods employed by other studies**
Posterior limb of the internal capsule	Chen et al. (2009) found no changes in FA or MD.	Pomara et al. (2001) found increased FA and no changes in MD.	*Pomara et al. (2001):* Direct measurements using manual ROI's. *Chen et al. (2009):* Parcellation of WM regions and voxel-based analysis.
Corpus callosum	Thurnher et al. (2005) found decreased FA and increased MD in the genu. Chen et al. (2009) found decreased FA in the genu. Wu et al. (2006) found decreased FA in the splenium.	Thurnher et al. (2005) found no FA or MD changes for the splenium. Chen et al. (2009) found increased MD in the genu and no changes in the body or splenium. Wu et al. (2006) found increased MD in the splenium and no changes in the genu.	*Thurnher et al. (2005):* Direct measurements using manual ROI's. *Wu et al. (2006):* Direct measurements using manual ROI's. *Chen et al. (2009):* Parcellation of WM regions and voxel-based analysis.
Corona radiata	Chen et al. (2009) found decreased FA in the anterior corona radiata and increased MD in the anterior and superior corona radiata.	Chen et al. (2009) found decreased FA in the superior and posterior corona radiata.	*Chen et al. (2009):* Parcellation of WM regions and voxel-based analysis.
Novel findings: sagittal stratum and cingulum	None	None	

5.2 Axial and radial diffusivity changes in HIV patients with and without apathy

Both TBSS and voxel-based DTI analyses have demonstrated differential changes in these two diffusivities for the HIV cohorts compared to the normal volunteers. Decreased AD was more widespread and significant than RD in both the non-apathetic and apathetic HIV groups. This gives insight into the pathological processes involved in HIV. As mentioned earlier, mouse studies have demonstrated that AD changes might be indicative of axonal damage and RD changes specific to demyelination (Song et al., 2002; Song et al., 2003; Song et al., 2005).

For the present study there were more widespread decreases in AD in the HIV apathetic cohort compared to healthy controls than when comparing the non-apathetic cohort to controls. AD decreases for both HIV cohorts were seen in regions of the internal capsule and corpus callosum, indicating that axonal damage occurs near striatal regions in early HIV infection. This is consistent with a model of HIV infection across the blood-brain barrier, in which HIV enters early in the infection phase and accumulates in the basal ganglia (Gonzalez-Scarano et al., 2005). Axial diffusivity decreases were also present in the external capsule and the cerebellar regions of the brain, which could implicate interference with motor function in HIV. This may also be related to the corticospinal tract FA decrease apparent in the HIV apathetic cohort. Motor impairments have been demonstrated in the advanced stages of HIV infection and HIV dementia (Ho et al., 1989).

Radial diffusivity is thought to be related to myelin integrity in disease processes, where increased RD and a constant AD correspond to decreased myelin integrity. Myelin degeneration has been identified as a major component of WM integrity loss in histopathological studies of HIV. For example, in HIV autopsy studies, diffuse WM damage was apparent in sections stained to detect myelin damage (Raja et al., 1997). A study by Gray et al., (1996) have also shown that even at the asymptomatic stage there is evidence of myelin pallor and gliosis in HIV patients. An interesting study measuring myelin in the CSF in HIV patients demonstrated a correlation with functional impairment in this population group (Liuzzi et al., 1992). The myelin protein levels were significantly higher in CSF for HIV patients with dementia than those with mild cognitive impairment and no protein levels were apparent in healthy controls and HIV patients without any functional impairment.

Increased RD was found for certain regions in the HIV non-apathetic cohort when compared to controls. This could indicate that myelin changes occur on a microstructural level even before it is detectable in CSF. Increased RD was detected across the corona radiata regions in the HIV apathetic cohort as well as in the corticospinal tract. This increased RD in the corticospinal tract could be due to the myelin damage that has occurred at the cerebellar level and once again could be an early marker of motor dysfunction in HIV.

5.3 Affected circuits implicating the reduced goal-directed behaviour in HIV apathy

The comparison between HIV subjects and healthy controls served to validate the methods of this study as comparisons could be made to previous studies. The main research focus of this study is, however, the WM correlates that are related to apathy in HIV. Therefore, the HIV non-apathetic cohort and the HIV apathetic cohort were compared.

The hypothesized FA decreases in the anterior thalamic radiation and the genu of the corpus callosum were detected in the apathy cohort. The anterior thalamic radiation connects the orbitofrontal lobe and the limbic system to the anterior and dorsomedial thalamic nuclei (Aralasmak et al., 2006). This is an integral connection in the frontal-subcortical circuits, which include the medial orbitofrontal and anterior cingulate circuits. Apathy has been observed in patients with neurodegenerative disorders presenting with lesions in the ventrolateral and dorsomedial thalamus (Levy et al., 2006). Lesions in the globus pallidus and internal capsule are also known to cause apathy (Aralasmak et al., 2006). In patients with Parkinson's disease (associated with decreased dopaminergic neurons), apathy has also been observed, especially in cases that involve the subcortical structures of the anterior cingulate circuit (Levy et al., 2006). The anterior cingulate has been shown to be responsible for goal-directed behaviour (Tekin et al., 2002). Perfusion studies in Alzheimer's disease have also correlated apathy with decreased anterior cingulate activity (Craig et al., 1996). Thus, the decreased FA in the thalamic radiation could indicate loss of connectivity in the anterior cingulate circuit. However it should be noted that no changes have been found in this structure for the other DTI metrics (AD, RD and MD), so the underlying physiological changes in axon density and myelin integrity remain unclear.

Decreased FA and increased MD were observed for the genu and body of the corpus callosum, indicating that there are recent inflammatory responses in this region, probably due

to the viral infection. The corpus callosum is a large bundle of WM fibers that are responsible for interhemispheric integration, and it provides connections with frontal cortices and striatal structures (Gazziniga, 2000). The anterior regions of the corpus callosum connect left and right frontal cortices, so a disruption in this relay system can impair hemisphere integration, thus also contributing to the dysfunction of frontal-striatal circuits. A study of cognitive dysfunction have shown that DTI measures in the corpus callosum are sensitive to subtle or early microstructural changes not always present on other types of MRI (Bozzali et al., 2002). In contrast to other studies of the CC where FA and MD changes were noted in the genu (Wu et al., 2006), this study identified changes in the splenium. Chang et al. (2008) conducted a prospective study examining the changes in FA and MD of an HIV cohort over a time period of one year and found increased diffusion in the genu of the CC compared to no significant diffusion changes in the splenium (Chang et al., 2008). Therefore there is evidence that the splenium and genu can be affected differently as is evident by the contrasting FA decrease in the genu and FA increase in the splenium.

5.4 Comparison of the processing techniques

Tract-based spatial statistics has certain theoretical advantages over a DTI analysis technique based on voxel-based morphometry (Smith et al., 2006). Most significantly, registration errors are less likely to occur by restricting the registration to the "skeleton" of the WM tracts than in an approach using all WM voxels. Another advantage of TBSS is the decreased search volume necessary for statistical comparison between groups. This in turn leads to a smaller multiple comparison problems and lends more statistical power to the study design. However, comparisons are restricted to the skeleton of WM and therefore TBSS is less sensitive to WM regions in close proximity to pathological grey matter regions. TBSS also requires more computational resources than the approach used in MATLAB, although this is not a limitation in practice. The two techniques use different methods of statistical inference, thus complicating a detailed comparison. TBSS uses a non-parametric permutation-based inference with threshold-free cluster enhancement, whereas the MATLAB approach uses general linear models. The AD changes that have been found in TBSS when comparing the HIV cohorts with the healthy controls indicate that TBSS might be more sensitive to detecting these changes than the voxel-based analysis.

There were no significant changes between the HIV apathetic cohort and the non-apathetic cohort for TBSS. However, when there was no correction for multiple comparisons in TBSS, similar results were noted compared to the voxel-based analysis (in fact, these were more widespread in TBSS). No significant changes were observed with the fiber tracking approach, but this is likely because DTI metrics were averaged across entire fiber bundles, which inherently decreases the sensitivity of the technique.

5.5. Limitations of diffusion tensor imaging

There are several limitations associated with DTI:

1) Axon directionality (afferent or efferent) cannot be determined from this contrast (Mori et al., 2006). Therefore it is difficult to ascertain whether the WM regions that demonstrate changes in HIV are projecting towards or away from cortical areas. The results from this study can only give an indication of which major WM tracts are affected.

2) Diffusion anisotropy is very sensitive to cellular level anatomy, but this is averaged over a large voxel volume containing multiple axonal fiber populations (the voxel size in this study was 1.9×1.9 mm^2, while an axon diameter is to the order of 10 μm). The varying orientations of multiple axons are averaged and therefore observations of diffusion anisotropy can only reliably be made if tissue structures within a voxel are homogenous both at a microscopic and macroscopic level. Therefore, any changes in anisotropy could be due to cellular structures such as axons and myelin, or due to varying macroscopic organization of the fibers. It is difficult to distinguish between the two possibilities (Mori et al., 2006).

3) DTI is sensitive to the motion of water which moves at a rate of 5-10 μm during the application of gradient pulses. If there are significant subject movements during a scan it can influence the results obtained by DTI. Because of the relatively long scanning time and noise levels associated with DTI sequences, subjects may have difficulty in remaining still for the duration of the scans, although certain hardware improvements and scanning multiple samples at a time can improve the acquisition (Bock et al., 2003).

5.6 Limitations of the data analysis techniques

Voxel-based analysis

The benefits of the VBM approach are that the analysis is fully automated, it is a whole-brain investigation and there is no need to define regions of interest (ROI). The approach is data driven which means that differences or abnormalities can be detected without prior information for any subject populations. However, this method also suffers from certain limitations:

1) Residual misalignment can influence the results from VBM, thus there is no guarantee that a specific voxel is from the same anatomical region across all subjects. One example of this is difference in ventricle size between group comparisons (for an example see the work by Simon et al. 2005). Other work shows FA results that are due to a shift in the pyramidal WM tracts rather than actual integrity differences (Vangberg et al., 2005). The neuroimaging community is aware of the problem and groups have been applying careful post-stats analyses. An example of this is to create a WM mask for a reported ROI in the statistical maps, and then examining whether the original image's anatomy corresponds with the findings (Sommer et al., 2002). Another method to obtain better registration results is to include additional information about the tensor in the registration process (Jones et al., 2002; Park et al., 2003). However, even a high degree of freedom (DOF) non-linear approach cannot guarantee optimal alignment between FA maps for different subjects.

2) Another common concern about VBM is the arbitrary way in which the amount of Gaussian smoothing is chosen. One option is to try a range of smoothing parameters, but then the final interpretation becomes more complex and this increases the amount of comparisons needed. However, for this study no smoothing was applied to the data.

Tract-based spatial statistics

Although TBSS is a more robust choice for analyzing diffusion data, it also suffers from certain technical limitations:

1) As with VBM, the confounding effects of head motion during a scan leads to increased blurring and FA data with false differences. Motion estimates from the preprocessing of the

data can be added as confounding regressors in the statistical model, but this can desensitize the model to significant differences (Smith et al., 2006).

2) Because of the low resolution of DTI images, some of the WM tracts are thinner than the actual voxel sizes and therefore it can be difficult to determine whether the change in FA is because of tract thickness change or actual changes within the tract. This is true for any voxel-based analysis as well. Thresholding the FA skeleton to exclude FA values below 0.2, as done in this study, improves this (Jones et al., 2005).

3) Interpreting the FA changes at WM tract crossings should also be done carefully. A reduction in FA could be because of an increase in tracts with lower FA that are feeding into the junction**,** rather than the higher FA tracts in the junction displaying actual decreased FA (Jones et al., 2005; Tuch et al., 2005).

6. Conclusions and recommendations

This study is the first to examine the co-morbid effects of apathy and HIV on the white matter microstructure of apathetic HIV^+ individuals.

The most significant findings were the decreases in WM integrity in frontal regions of HIV patients presenting with apathy. These regions are associated with frontal-striatal circuits, specifically circuits involved in motivational behavior. Decreased WM integrity in these regions could be responsible for the apathetic syndrome observed in these patients and therefore can contribute as evidence to the neurobiological models of apathy as seen in other neurological and neurodegenerative disorders. In addition, explanations for possible physiological changes in WM have also been elucidated by examining the AD and RD between groups. Widespread decreases in AD relative to less widespread increases in RD were evident for HIV patients. This suggests that axonal damage might be the primary pathological process with demyelination as a secondary process demonstrated by increases in RD. Apathy-specific changes were also apparent in frontal WM and the corpus callosum, suggesting that these structures could be possible bio-markers for apathy.

Given that diffusion tensor imaging and data analysis is a developing science, a number of techniques for analyzing data were applied in this study. There were several differences between data outputs when comparing the techniques. TBSS is seemingly a more robust method for analyzing DTI data, as it addresses some of the fundamental problems of voxel-based techniques. Fiber tracking could also be potentially useful, but perhaps not in the way it was applied here, i.e. assessing average FA values across whole tracts.

To assess the validity of these findings, a prospective study is required to measure changes in DTI metrics over time. This is also important to establish whether the changes seen here are reversible or indicative of permanent injury to WM. The brain has the capacity for functional reorganization and it would be interesting to observe whether this holds true for patients with HIV apathy as well. Also, observing DTI data on its own only provides a limited observation of brain changes in HIV as well as apathy. It would be beneficial to examine the frontal-striatal circuits in more detail by incorporating information from additional imaging techniques. For example, data from fMRI studies in HIV and associated co-morbidities can be used as markers of abnormal activity in cortices of interest, such as the anterior cingulate and

motor cortex. Volume changes in these cortices and the corresponding basal ganglia grey matter could also be measured using structural analysis techniques such as voxel-based morphometry or cortical thickness mapping. By applying DTI tractography, tracts that connect to the regions presenting with functional and structural deficit can be mapped and global DTI changes can be examined. Also by applying voxel-based techniques such as TBSS in these white matter regions, smaller WM microstructural changes can be detected and examined.

References

1. **Adle-Biassette H, Chretien F, Wingertsmann L, Hery C, Ereau T, Scaravilli F, Tardieu M, and Gray F**. Neuronal apoptosis does not correlate with dementia in HIV infection but is related to microglial activation and axonal damage. *Neuropathol Appl Neurobiol* 25: 123-133, 1999.

2. **Anderson E, Zink W, Xiong H, and Gendelman HE**. HIV-1-associated dementia: a metabolic encephalopathy perpetrated by virus-infected and immune-competent mononuclear phagocytes. *J Acquir Immune Defic Syndr* 31 Suppl 2: S43-54, 2002.

3. **Andersson JL, and Skare S.** A model-based method for retrospective correction of geometric distortions in diffusion-weighted EPI. *Neuroimage* 16:177-199, 2002

4. **Andreasen NC**. Negative symptoms in schizophrenia. *Arch Gen Psychiatry* 39:784-794, 1982

5. **Aralasmak A, Ulmer JL, Kocak M, Salvan CV, Hillis AE, and Yousem DM**. Association, commisural, and projection pathways and their functional deficit reported in literature. *J Comput Assist Tomogr* 30: 695-715, 2006

6. **Assaf Y, and Pasternak O**. Diffusion tensor imaging (DTI)-based white matter mapping in brain research: a review. *J Mol Neurosci* 34:51-61, 2008

7. **Ashburner J, and Friston KJ**. Voxel-based morphometry--the methods. *Neuroimage* 11: 805-821, 2000.

8. **Bagasra O, Lavi E, Bobroski L, Khalili K, Pestaner JP, Tawadros R, and Pomerantz RJ**. Cellular reservoirs of HIV-1 in the central nervous system of infected individuals: identification by the combination of in situ polymerase chain reaction and immunohistochemistry. *AIDS* 10: 573-585, 1996.

9. **Basser PJ, and Jones DK**. Diffusion-tensor MRI: theory, experimental design and data analysis - a technical review. *NMR Biomed* 15: 456-467, 2002.

10. **Basser PJ, Mattiello J, and LeBihan D**. MR diffusion tensor spectroscopy and imaging. *Biophys J* 66: 259-267, 1994.

11. **Beaulieu C**. The basis of anisotropic water diffusion in the nervous system - a technical review. *NMR Biomed* 15: 435-455, 2002.

12. **Beaulieu C, and Allen PS**. Determinants of anisotropic water diffusion in nerves. *Magn Reson Med* 31: 394-400, 1994.

13. **Berghuis JP, Uldall KK, and Lalonde B**. Validity of two scales in identifying HIV-associated dementia. *J Acquir Immune Defic Syndr* 21: 134-140, 1999.

14. **Bozzali M, Falini A, Franceschi M, Cercignani M, Zuffi M, Scotti G, Comi G, and Filippi M**. White matter damage in Alzheimer's disease assessed in vivo using diffusion tensor magnetic resonance imaging. *J Neurol Neurosurg Psychiatry* 72 (6):742-746, 2002.

15. **Brown RG, and Pluck G**. Negative symptoms: the 'pathology' of motivation and goal-directed behaviour. *Trends Neurosci* 23: 412-417, 2000

16. **Budde MD, Kim JH, Liang HF, Schmidt RE, Russell JH, Cross AH, and Song SK**. Toward accurate diagnosis of white matter pathology using diffusion tensor imaging. *Magn Reson Med* 57: 688-695, 2007.

17. **Buki A, Okonkwo DO, Wang KK, and Povlishock JT**. Cytochrome c release and caspase activation in traumatic axonal injury. *J Neurosci* 20: 2825-2834, 2000.

18. **Castellon SA, Hinkin CH, and Myers HF**. Neuropsychiatric disturbance is associated with executive dysfunction in HIV-1 infection. *J Int Neuropsychol Soc* 6: 336-347, 2000.

19. **Castellon SA, Hinkin CH, Wood S, and Yarema KT**. Apathy, depression, and cognitive performance in HIV-1 infection. *J Neuropsychiatry Clin Neurosci* 10: 320-329, 1998.

20. **Catani M, Howard RJ, Pajevic S, and Jones DK**. Virtual in vivo interactive dissection of white matter fasciculi in the human brain. *Neuroimage* 17: 77-94, 2002.

21. **Chang L, Wong V, Nakama H, Watters M, Ramones D, Miller EN, Cloak C, and Ernst T**. Greater than age-related changes in brain diffusion of HIV patients after 1 year. *J Neuroimmune Pharmacol* 3 (4):265-274, 2008

22. **Chen Y, An H, Zhu H, Stone T, Smith JK, Hall C, Bullitt E, Shen D, Lin W.** White matter abnormalities revealed by diffusion tensor imaging in non-demented and demented HIV+ patients. *Neuroimage* 10.1016/j.neuroimage.2009.04.030

23. **Chukwudelunzu FE, Meschia JF, Graff-Radford NR, and Lucas JA**. Extensive metabolic and neuropsychological abnormalities associated with discrete infarction of the genu of the internal capsule. *J Neurol Neurosurg Psychiatry* 71: 658-662, 2001.

24. **Cloak CC, Chang L, and Ernst T**. Increased frontal white matter diffusion is associated with glial metabolites and psychomotor slowing in HIV. *J Neuroimmunol* 157: 147-152, 2004.

25. **Conturo TE, Lori NF, Cull TS, Akbudak E, Snyder AZ, Shimony JS, McKinstry RC, Burton H, and Raichle ME**. Tracking neuronal fiber pathways in the living human brain. *Proc Natl Acad Sci U S A* 96: 10422-10427, 1999.

26. **Craig AH, Cummings JL, Fairbanks L, Itti L, Miller BL, Li J, and Mena I**. Cerebral blood flow correlates of apathy in Alzheimer disease. *Arch Neurol* 53(11): 1116-1120, 1996

27. **Filippi CG, Ulug AM, Ryan E, Ferrando SJ, and van Gorp W**. Diffusion tensor imaging of patients with HIV and normal-appearing white matter on MR images of the brain. *AJNR Am J Neuroradiol* 22: 277-283, 2001.

28. **Giulian D, Vaca K, and Corpuz M**. Brain glia release factors with opposing actions upon neuronal survival. *J Neurosci* 13: 29-37, 1993.

29. **Gonzalez-Scarano F, and Martin-Garcia J**. The neuropathogenesis of AIDS. *Nat Rev Immunol* 5: 69-81, 2005.

30. **Good CD, Johnsrude IS, Ashburner J, Henson RN, Friston KJ, and Frackowiak RS**. A voxel-based morphometric study of ageing in 465 normal adult human brains. *Neuroimage* 14: 21-36, 2001.

31. **Gorry PR, Ong C, Thorpe J, Bannwarth S, Thompson KA, Gatignol A, Vesselingh SL, and Purcell DF**. Astrocyte infection by HIV-1: mechanisms of restricted virus replication, and role in the pathogenesis of HIV-1-associated dementia. *Curr HIV Res* 1: 463-473, 2003.

32. **Gray F, Belec L, Chretien F, Dubreuil-Lemaire ML, Ricolfi F, Wingertsmann L, Poron F, and Gherardi R**. Acute, relapsing brain oedema with diffuse blood-brain barrier alteration and axonal damage in the acquired immunodeficiency syndrome. *Neuropathol Appl Neurobiol* 24: 209-216, 1998.

33. **Gulani V, Webb AG, Duncan ID, and Lauterbur PC**. Apparent diffusion tensor measurements in myelin-deficient rat spinal cords. *Magn Reson Med* 45: 191-195, 2001.

34. **Haase AT**. Pathogenesis of lentivirus infections. *Nature* 322: 130-136, 1986.

35. **Hall DE, Moffat BA, Stojanovska J, Johnson TD, Li Z, Hamstra DA, Rehemtulla A, Chenevert TL, Carter J, Pietronigro D, and Ross BD**. Therapeutic efficacy of DTI-015 using diffusion magnetic resonance imaging as an early surrogate marker. *Clin Cancer Res* 10: 7852-7859, 2004.

36. **Hamilton M**. A rating scale for depression. *J Neurol Neurosurg Psychiatry* 23: 56-62, 1960.

37. **Hinkin CH, Castellon SA, Atkinson JH, and Goodkin K**. Neuropsychiatric aspects of HIV infection among older adults. *J Clin Epidemiol* 54 Suppl 1: S44-52, 2001.

38. **Ho DD, Bredesen DE, Vinters HV, and Daar ES**. The acquired immunodeficiency syndrome (AIDS) dementia complex. *Ann Intern Med* 111: 400-410, 1989.

39. **Hofer S, and Frahm J**. Topography of the human corpus callosum revisited--comprehensive fiber tractography using diffusion tensor magnetic resonance imaging. *Neuroimage* 32: 989-994, 2006.

40. **Jiang H, van Zijl PC, Kim J, Pearlson GD, and Mori S**. DtiStudio: resource program for diffusion tensor computation and fiber bundle tracking. *Comput Methods Programs Biomed* 81: 106-116, 2006.

41. **Kaul M, Garden GA, and Lipton SA**. Pathways to neuronal injury and apoptosis in HIV-associated dementia. *Nature* 410: 988-994, 2001.

42. **Kramer-Hammerle S, Rothenaigner I, Wolff H, Bell JE, and Brack-Werner R**. Cells of the central nervous system as targets and reservoirs of the human immunodeficiency virus. *Virus Res* 111: 194-213, 2005.

43. **Langford D, and Masliah E**. Crosstalk between components of the blood brain barrier and cells of the CNS in microglial activation in AIDS. *Brain Pathol* 11: 306-312, 2001.

44. **Lawrence DM, and Major EO**. HIV-1 and the brain: connections between HIV-1-associated dementia, neuropathology and neuroimmunology. *Microbes Infect* 4: 301-308, 2002.

45. **Le Bihan D, Breton E, Lallemand D, Grenier P, Cabanis E, and Laval-Jeantet M**. MR imaging of intravoxel incoherent motions: application to diffusion and perfusion in neurologic disorders. *Radiology* 161: 401-407, 1986.

46. **Levy R, and DuBois B**. Apathy and the functional anatomy of the prefrontal cortex-basal ganglia circuits. *Cerebral Cortex* 16: 916 – 928, 2006

47. **Liuzzi GM, Mastroianni CM, Vullo V, Jirillo E, Delia S, Riccio P**. Cerebrospinal fluid myelin basic protein as predictive marker of demyelination in AIDS dementia complex. *J Neuroimmunol* 36: 251-254, 1992

48. **Llacer J**. Tomographic image reconstruction by eigenvector decomposition: its limitations and areas of applicability. *IEEE Trans Med Imaging* 1: 34-42, 1982.

49. **LoPachin RM, Jr., and Lehning EJ**. Acrylamide-induced distal axon degeneration: a proposed mechanism of action. *Neurotoxicology* 15: 247-259, 1994.

50. **Lopez OL, Zivkovic S, Smith G, Becker JT, Meltzer CC, and DeKosky ST**. Psychiatric symptoms associated with cortical-subcortical dysfunction in Alzheimer's disease. *J Neuropsychiatry Clin Neurosci* 13: 56-60, 2001.

51. **Madureira S, Guerreiro M, and Ferro JM**. A follow-up study of cognitive impairment due to inferior capsular genu infarction. *J Neurol* 246: 764-769, 1999.

52. **Mankowski JL, Queen SE, Tarwater PM, Fox KJ, and Perry VH**. Accumulation of beta-amyloid precursor protein in axons correlates with CNS expression of SIV gp41. *J Neuropathol Exp Neurol* 61: 85-90, 2002.

53. **Marin RS**. Differential diagnosis and classification of apathy. *Am J Psychiatry* 147: 22-30, 1990.

54. **Marin RS, Biedrzycki RC, and Firinciogullari S**. Reliability and validity of the Apathy Evaluation Scale. *Psychiatry Res* 38: 143-162, 1991.

55. **McGilchrist I, Goldstein LH, Jadresic D, and Fenwick P**. Thalamo-frontal psychosis. *Br J Psychiatry* 163: 113-115, 1993.

56. **Migneco O, Benoit M, Koulibaly PM, Dygai I, Bertogliati C, Desvignes P, Robert PH, Malandain G, Bussiere F, and Darcourt J**. Perfusion brain SPECT and statistical parametric mapping analysis indicate that apathy is a cingulate syndrome: a study in Alzheimer's disease and nondemented patients. *Neuroimage* 13: 896-902, 2001.

57. **Mori S, and Barker PB**. Diffusion magnetic resonance imaging: its principle and applications. *Anat Rec* 257: 102-109, 1999.

58. **Mori S, and Zhang J**. Principles of diffusion tensor imaging and its applications to basic neuroscience research. *Neuron* 51: 527-539, 2006.

59. **Moroni M, and Antinori S**. HIV and direct damage of organs: disease spectrum before and during the highly active antiretroviral therapy era. *AIDS* 17 Suppl 1: S51-64, 2003.

60. **Moseley ME, Cohen Y, Mintorovitch J, Chileuitt L, Shimizu H, Kucharczyk J, Wendland MF, and Weinstein PR**. Early detection of regional cerebral ischemia in cats: comparison of diffusion- and T2-weighted MRI and spectroscopy. *Magn Reson Med* 14: 330-346, 1990.

61. **Neil JJ**. Diffusion imaging concepts for clinicians. *J Magn Reson Imaging* 27: 1-7, 2008.

62. **Neumann M, Afonina E, Ceccherini-Silberstein F, Schlicht S, Erfle V, Pavlakis GN, and Brack-Werner R**. Nucleocytoplasmic transport in human astrocytes: decreased nuclear uptake of the HIV Rev shuttle protein. *J Cell Sci* 114: 1717-1729, 2001.

63. **Nuovo GJ, Becker J, Burk MW, Margiotta M, Fuhrer J, and Steigbigel RT**. In situ detection of PCR-amplified HIV-1 nucleic acids in lymph nodes and peripheral blood in patients with asymptomatic HIV-1 infection and advanced-stage AIDS. *J Acquir Immune Defic Syndr* 7: 916-923, 1994.

64. **Okada K, Kobayashi S, Yamagata S, Takahashi K, and Yamaguchi S**. Poststroke apathy and regional cerebral blood flow. *Stroke* 28: 2437-2441, 1997.

65. **Ott BR, Noto RB, and Fogel BS**. Apathy and loss of insight in Alzheimer's disease: a SPECT imaging study. *J Neuropsychiatry Clin Neurosci* 8:41-46, 1996

66. **Papoulis A.** Probability, Random Variables, and Stochastic Processes (3rd ed). *McCraw-Hill, Inc.*

67. **Paul RH, Brickman AM, Navia B, Hinkin C, Malloy PF, Jefferson AL, Cohen RA, Tate DF, and Flanigan TP**. Apathy is associated with volume of the nucleus accumbens in patients infected with HIV. *J Neuropsychiatry Clin Neurosci* 17: 167-171, 2005.

68. **Pierpaoli C, and Basser PJ**. Toward a quantitative assessment of diffusion anisotropy. *Magn Reson Med* 36: 893-906, 1996.

69. **Phillips ML, Drevets WC, Rauch SL, Lane R.** Neurobiology of emotion perception II: implications for major psychiatric disorders. *Biol Psychiatry* 54: 515-528, 2003

70. **Pomara N, Crandall DT, Choi SJ, Johnson G, and Lim KO**. White matter abnormalities in HIV-1 infection: a diffusion tensor imaging study. *Psychiatry Res* 106: 15-24, 2001.

71. **Rabkin JG, Ferrando SJ, van Gorp W, Rieppi R, McElhiney M, and Sewell M**. Relationships among apathy, depression, and cognitive impairment in HIV/AIDS. *J Neuropsychiatry Clin Neurosci* 12: 451-457, 2000.

72. **Ragin AB, Storey P, Cohen BA, Epstein LG, and Edelman RR**. Whole brain diffusion tensor imaging in HIV-associated cognitive impairment. *AJNR Am J Neuroradiol* 25: 195-200, 2004.

73. **Ragin AB, Wu Y, Storey P, Cohen BA, Edelman RR, Epstein LG**. Diffusion tensor imaging of subcortical brain injury in patients infected with human immunodeficiency virus. *J Neurovirol* 11: 292-298

74. **Raja F, Sherriff FE, Morris CS, Bridges LR, and Esiri MM**. Cerebral white matter damage in HIV infection demonstrated using beta-amyloid precursor protein immunoreactivity. *Acta Neuropathol* 93: 184-189, 1997.

75. **Saito Y, Matsumura K, and Shimizu T**. Anterograde amnesia associated with infarction of the anterior fornix and genu of the corpus callosum. *J Stroke Cerebrovasc Dis* 15: 176-177, 2006.

76. **Sakuma H, Nomura Y, Takeda K, Tagami T, Nakagawa T, Tamagawa Y, Ishii Y, and Tsukamoto T**. Adult and neonatal human brain: diffusional anisotropy and myelination with diffusion-weighted MR imaging. *Radiology* 180: 229-233, 1991.

77. **Sheehan DV, Lecrubier Y, Sheehan KH, Amorim P, Janavs J, Weiller E, Hergueta T, Baker R, and Dunbar GC**. The Mini-International Neuropsychiatric Interview (M.I.N.I.): the development and validation of a structured diagnostic psychiatric interview for DSM-IV and ICD-10. *J Clin Psychiatry* 59 Suppl 20: 22-33;quiz 34-57, 1998.

78. **Smith SM, Jenkinson M, Johansen-Berg H, Rueckert D, Nichols TE, Mackay CE, Watkins KE, Ciccarelli O, Cader MZ, Matthews PM, and Behrens TE**. Tract-based spatial statistics: voxelwise analysis of multi-subject diffusion data. *Neuroimage* 31: 1487-1505, 2006.

79. **Song SK, Sun SW, Ju WK, Lin SJ, Cross AH, and Neufeld AH**. Diffusion tensor imaging detects and differentiates axon and myelin degeneration in mouse optic nerve after retinal ischemia. *Neuroimage* 20: 1714-1722, 2003.

80. **Song SK, Sun SW, Ramsbottom MJ, Chang C, Russell J, and Cross AH**. Dysmyelination revealed through MRI as increased radial (but unchanged axial) diffusion of water. *Neuroimage* 17: 1429-1436, 2002.

81. **Song SK, Yoshino J, Le TQ, Lin SJ, Sun SW, Cross AH, and Armstrong RC**. Demyelination increases radial diffusivity in corpus callosum of mouse brain. *Neuroimage* 26: 132-140, 2005.

82. **Sorensen AG, Wu O, Copen WA, Davis TL, Gonzalez RG, Koroshetz WJ, Reese TG, Rosen BR, Wedeen VJ, and Weisskoff RM**. Human acute cerebral ischemia: detection of changes in water diffusion anisotropy by using MR imaging. *Radiology* 212: 785-792, 1999.

83. **Sotak CH**. The role of diffusion tensor imaging in the evaluation of ischemic brain injury - a review. *NMR Biomed* 15: 561-569, 2002.

84. **Starkstein SE, Mayberg HS, Preziosi TJ, Andrezejewski P, Leiguarda R, and Robinson RG**. Reliability, validity, and clinical correlates of apathy in Parkinson's disease. *J Neuropsychiatry Clin Neurosci* 4 (2): 134-139, 1992

85. **Stebbins GT, Smith CA, Bartt RE, Kessler HA, Adeyemi OM, Martin E, Cox JL, Bammer R, and Moseley ME**. HIV-associated alterations in normal-appearing white matter: a voxel-wise diffusion tensor imaging study. *J Acquir Immune Defic Syndr* 46: 564-573, 2007.

86. **Stieltjes B, Kaufmann WE, van Zijl PC, Fredericksen K, Pearlson GD, Solaiyappan M, and Mori S**. Diffusion tensor imaging and axonal tracking in the human brainstem. *Neuroimage* 14: 723-735, 2001.

87. **Talairach J, and Tournoux P**. Referentially oriented cerebral MRI anatomy: An atlas of stereotaxic anatomical correlations for gray and white matter *Thieme Medical Publishers, New York*, 1993

88. **Thurnher MM, Castillo M, Stadler A, Rieger A, Schmid B, and Sundgren PC**. Diffusion-tensor MR imaging of the brain in human immunodeficiency virus-positive patients. *AJNR Am J Neuroradiol* 26: 2275-2281, 2005.

89. **Tekin S, and Cummings JL**. Frontal-subcortical neuronal circuits and clinical neuropsychiatry: An update *J Psychosom Res* 53: 647-654, 2002

90. **van Reekum R, Stuss DT, and Ostrander L**. Apathy: why care? *J Neuropsychiatry Clin Neurosci* 17: 7-19, 2005.

91. **Wakana S, Caprihan A, Panzenboeck MM, Fallon JH, Perry M, Gollub RL, Hua K, Zhang J, Jiang H, Dubey P, Blitz A, van Zijl P, and Mori S**. Reproducibility of quantitative tractography methods applied to cerebral white matter. *Neuroimage* 36: 630-644, 2007.

92. **Wang KK, Posmantur R, Nadimpalli R, Nath R, Mohan P, Nixon RA, Talanian RV, Keegan M, Herzog L, and Allen H**. Caspase-mediated fragmentation of calpain inhibitor protein calpastatin during apoptosis. *Arch Biochem Biophys* 356: 187-196, 1998.

93. **Watanabe MD, Martin EM, DeLeon OA, Gaviria M, Pavel DG, and Trepashko DW**. Successful methylphenidate treatment of apathy after subcortical infarcts. *J Neuropsychiatry Clin Neurosci* 7: 502-504, 1995.

94. **Werring DJ, Toosy AT, Clark CA, Parker GJ, Barker GJ, Miller DH, and Thompson AJ**. Diffusion tensor imaging can detect and quantify corticospinal tract degeneration after stroke. *J Neurol Neurosurg Psychiatry* 69: 269-272, 2000.

95. **Wimberger DM, Roberts TP, Barkovich AJ, Prayer LM, Moseley ME, and Kucharczyk J**. Identification of "premyelination" by diffusion-weighted MRI. *J Comput Assist Tomogr* 19: 28-33, 1995.

96. **Witelson SF**. Hand and sex differences in the isthmus and genu of the human corpus callosum. A postmortem morphological study. *Brain* 112 (Pt 3): 799-835, 1989.

97. **Wu Y, Storey P, Cohen BA, Epstein LG, Edelman RR, Ragin AB.** Diffusion alterations in corpus callosum of patients with HIV. *Am J Neuroradiol* 27: 656-660

98. **Xue R, van Zijl PC, Crain BJ, Solaiyappan M, and Mori S**. In vivo three-dimensional reconstruction of rat brain axonal projections by diffusion tensor imaging. *Magn Reson Med* 42: 1123-1127, 1999.

Addendum A: Tractography results

Anterior thalamic radiation (ATR)

Table A1 shows the tractography results for the ATR. The statistical analysis was performed in SPSS 16.0. Even though no significant differences were found for either of the 3 group comparisons at $p < 0.05$, certain trends were apparent. Because FA and MD were averaged over the entire tract, smaller voxel changes will be masked by the variability present in different regions of the tract. Examining the trends, there was a non-significant FA decrease and MD increase in the left and right anterior thalamic radiations for the HIV apathetic cohort when compared to the HIV non-apathetic cohort. This corresponds to the right hemispheric decrease in ATR FA that was found in the voxel-based analysis. Contrasting trends were present in the right and left ATR when comparing the healthy control cohort to the respective HIV cohorts. Non-significant FA decreases and MD increases in the right ATR were found for both HIV cohorts compared to a healthy control cohort. However non-significant increases in FA and subsequent decreases in MD were present in the left ATR for the two HIV cohorts.

Table A1: Tractography results for the anterior thalamic radiation. Shown here are the FA and MD global changes in the anterior thalamic radiation for each comparison. An independent sample t-test was performed for each group comparison in the statistical package SPSS 16.0.

Analysis	Mean FA (SD)	Mean MD (SD)	p-value
HIV non-apathetic (n=13) vs HIV apathetic (n=13)	HIV non-apathetic ATR (R): 0.464 (0.017) ATR (L): 0.475 (0.020) HIV apathetic ATR (R): 0.461 (0.022) ATR (L) 0.473 (0.024)	HIV non-apathetic ATR (R): $7.43x10^{-4}$ ($3.27x10^{-5}$) ATR (L): $7.46x10^{-4}$ ($2.77x10^{-5}$) HIV apathetic ATR (R): $7.50x10^{-4}$ ($1.80x10^{-5}$) ATR (L): $7.53x10^{-4}$ ($1.50x10^{-5}$)	ATR (R) FA: 0.734 ATR (L) FA: 0.820 ATR (R) MD: 0.509 ATR (L) MD: 0.408
Healthy controls (n=10) vs HIV apathetic (n=13)	Healthy controls ATR (R): 0.465 (0.017) ATR (L): 0.461 (0.012) HIV apathetic ATR (R): 0.461 (0.022) ATR (L) 0.473 (0.024)	Healthy controls ATR (R): $7.47x10^{-4}$ ($2.81x10^{-5}$) ATR (L): $7.42x10^{-4}$ ($2.47x10^{-5}$) HIV apathetic ATR (R): $7.50x10^{-4}$ ($1.80x10^{-5}$) ATR (L): $7.53x10^{-4}$ ($1.50x10^{-5}$)	ATR (R) FA: 0.641 ATR (L) FA: 0.155 ATR (R) MD: 0.716 ATR (L) MD: 0.237
Healthy controls (n=10) vs HIV non-apathetic (n=13)	Healthy controls ATR (R): 0.465 (0.017) ATR (L): 0.461 (0.012) HIV non-apathetic ATR (R): 0.464 (0.017) ATR (L): 0.475 (0.020)	Healthy controls ATR (R): $7.47x10^{-4}$ ($2.81x10^{-5}$) ATR (L): $7.42x10^{-4}$ ($2.47x10^{-5}$) HIV non-apathetic ATR (R): $7.43x10^{-4}$ ($3.27x10^{-5}$) ATR (L): $7.46x10^{-4}$ ($2.77x10^{-5}$)	ATR (R) FA: 0.872 ATR (L) FA: 0.055 ATR (R) MD: 0.807 ATR (L) MD: 0.750

Corpus callosum

Table 7.2 shows the mean FA values for each cohort. The statistical analysis was performed in SPSS 16.0. An independent sample t-test was performed for each of the 3 group comparisons, but no significant differences were found at $p < 0.05$. When examining the trends, there were non-significant decreases in FA for each functional region in the HIV non-apathetic cohort compared to a healthy control cohort. However, non-significant increases in FA were found in the anterior and posterior midbody regions for the HIV apathetic cohort compared to the healthy control cohort. This is in contrast to the TBSS findings which have shown significant decreased FA in the CC body region.

Table A2: Summary of corpus callosum FA means (SD) for functional regions. This table is a summary of the FA means and standard deviations for the five functional regions according to Hofer and Frahm (2006). Each region corresponds to a functional region in both hemispheres of the brain. An independent sample t-test was performed for each group comparison at $p < 0.05$.

Cohort	**Region 1:** **Prefrontal**	**Region 2:** **Premotor and supplementary motor**	**Region 3:** **Primary motor**	**Region 4:** **Primary sensory**	**Region 5:** **Parietal, temporal and visual**
Healthy controls (n=10)	0.484 (0.034)	0.484 (0.044)	0.481 (0.031)	0.480 (0.040)	0.533 (0.032)
HIV non-apathetic (n=13)	0.464 (0.069)	0.468 (0.062)	0.470 (0.063)	0.452 (0.059)	0.521 (0.050)
HIV apathetic (n=13)	0.472 (0.025)	0.486 (0.026)	0.483 (0.042)	0.455 (0.050)	0.531 (0.031)